MICROWAVE FERRITE MATERIALS

In microwave technology it is often necessary to eliminate or reduce the unwanted interaction between different parts of a circuit or component. This function is generally realized with the help of a certain class of magnetic materials known as ferrites, which consist of mixed oxides of iron and other metals. Ferrites have many applications in other fields of technology, such as magnetic recording, memory devices, and permanent magnets, but in this article we will focus on those materials that have been found to be useful in microwave applications. The most important of these applications is arguably their use in nonreciprocal devices, such as circulators and isolators, which reduce the unwanted interaction between different parts of a circuit. In addition, these materials have also been used extensively in signal control devices, such as phase shifters, filters, switches, delay lines, and variable attenuators.

Microwave ferrites have substantially the same chemical composition as the ferrites used in other applications, but in many cases special, high-purity compositions are required, and exceptionally strict process control is necessary, in order to achieve good performance.

OVERVIEW: MICROWAVE BEHAVIOR OF FERRITE MATERIALS

Ferrites owe their unique utility in microwave technology primarily to two factors: They are electrical insulators, and the phenomenon of ferromagnetic resonance (FMR) provides for

J. Webster (ed.), *Wiley Encyclopedia of Electrical and Electronics Engineering*. Copyright © 1999 John Wiley & Sons, Inc.

nonreciprocal behavior and for tunability, as will be explained further. The classical ferromagnetic materials, such as iron, cobalt, nickel, and their alloys, also exhibit FMR, but because of their high electrical conductivity, an electromagnetic field penetrates only a very short distance (typically about 1 μm) into these materials at microwave frequencies, thus rendering them far less useful for microwave applications.

Brief History of Ferrites and Ferrimagnetism

Although one particular type of ferrite, magnetite Fe_3O_4, has been known since antiquity, their development into technologically useful materials is of relatively recent date. Important basic research was performed in the 1930s, and a theoretical model for these materials was created by Néel (1), who received the Nobel prize in Physics in 1970 for this work. The development of technologically useful materials occurred in the 1940s, mostly at the Philips Research Laboratories under the guidance of Snoek (2), Verwey, and Wijn (3). Pioneering work on the application of ferrites in microwave technology was done by Hogan (4) at Bell Telephone Laboratories.

The spontaneous magnetic moment of all magnetic materials can generally be attributed to the spin angular momentum of the electrons contained in the material, with the orbital angular momentum contributing relatively little by comparison. Oxide materials, such as ferrites, can be understood as consisting of positively charged metal ions, and negatively charged oxygen ions, all arranged in an orderly lattice. The oxygen ions do not contribute to the magnetic moment of the material, because they contain only completely filled shells of electrons, in which the spin angular momenta cancel each other. The metal ions, however, contain partially filled electron shells, which contribute to the net angular momentum of each ion according to well-established rules [see for instance Smit and Wijn (3) and Kittel (5)]. Néel's key insight was to note that the interaction between the metal ions of the lattice, the so-called *exchange interaction,* often favors antiparallel alignment of the spin angular momenta of adjacent ions. In some materials this leads to complete cancellation of the net magnetic moment. Such materials are said to be *antiferromagnetic.* In the ferrites the cancellation is only partial, so that a significant net magnetic moment remains. Such materials are said to be *ferrimagnetic,* to distinguish them from ordinary ferromagnetic materials, in which all moments are aligned parallel.

Electron Spin Resonance and Gyromagnetic Properties

The magnetic moment $\boldsymbol{M}$ of an electron is proportional to its spin angular momentum $\boldsymbol{J}$.

$$\boldsymbol{M} = -\gamma \boldsymbol{J} \qquad \gamma = g(e/2mc) \tag{1}$$

where the gyromagnetic ratio γ is defined as positive. Equation (1) is expressed in terms of the magnitude of the electron's charge (e) and mass (m), the light velocity (c), and the spectroscopic splitting factor (g), a number close to 2. Equation (1) also applies to the magnetic moment and angular momentum of each metal ion in the ferrite lattice, and by extension, to the magnetic moment and angular momentum of any macroscopic sample of the ferrite material. If the material is exposed to a magnetic field characterized by the vector $\boldsymbol{H}$, a torque is generated that has magnitude and direction given by the vector product $\mu_0 \boldsymbol{M} \times \boldsymbol{H}$, where μ_0 is the permeability of vacuum. Since the rate of change of angular momentum must equal the torque, the magnetic moment obeys the equation of motion shown in Fig. 1 (lower left). This equation also applies when $\boldsymbol{M}$ is interpreted to be the magnetic moment per unit volume, the magnetization. It should be understood, however, that damping (dissipation) is not included in this preliminary consideration. Figure 1 also illustrates the solution of the equation of motion. The magnetization vector moves around the direction of constant magnetic field $\boldsymbol{H}_0$, in a manner analogous to the motion of a spinning top or gyroscope in the earth's gravitational field. This motion is referred to as *spin precession.*

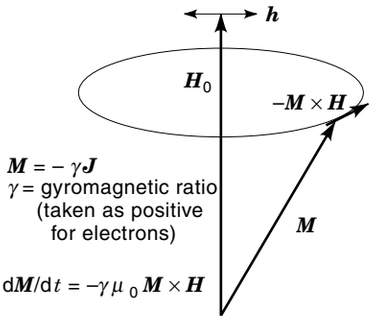

Figure 1. Gyromagnetic response of dc-biased ferrite to RF magnetic field (without damping).

The angular frequency of the precession motion is given by the product of $\gamma\mu_0$ and $\boldsymbol{H}_0 = |\boldsymbol{H}_0|$. If a small RF field $\boldsymbol{h}$ is present in addition to the constant field $\boldsymbol{H}_0$ (see Fig. 1), and if the frequency of this RF field coincides with the precession frequency, the amplitude of the spin precession will grow indefinitely in the absence of dissipation. This is the phenomenon of electron spin resonance. For ferro- or ferrimagnetic materials this resonance is referred to as ferromagnetic resonance or FMR.

The gyromagnetic properties of ferrites, qualitatively illustrated in Fig. 1, imply that an RF magnetic field applied in the x-direction (perpendicular to the z-direction, the direction of the dc bias field) will induce a magnetization response in the y-direction. Other articles in this encyclopedia discuss how this behavior is used in the realization of nonreciprocal components for microwave circuits. It is also readily apparent that FMR can be used to realize signal control devices, since the material behavior can be modified by changing the strength of the dc bias field.

Classes of Ferrite Materials

The technologically important ferrites can be classified according to their crystal structure as being either spinel, garnet, or hexagonal. The spinel-ferrite has the same crystal structure as the mineral spinel ($MgAl_2O_4$) and the garnet-ferrite is analogous to the mineral garnet ($Mn_3Al_2Si_3O_{12}$). The hexagonal ferrites (also called hexa-ferrite) have much in common with the spinel-ferrites, since they can be considered to consist of spinel-like layers that are stacked along the [111] direction of the spinel lattice and interspersed periodically with modified layers that contain elements from the second column of the periodic table, usually Ba or Sr.

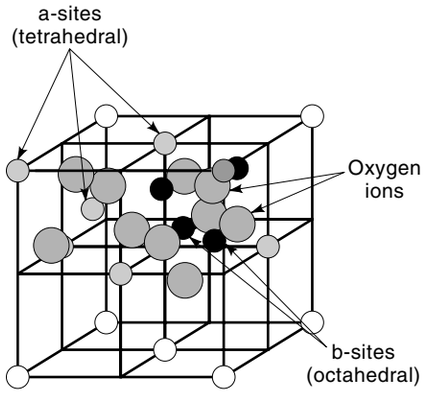

Figure 2. Spinel crystal structure: Two formula units are contained in the highlighted two octants of the unit cell.

For a more detailed review of the science and technology of microwave ferrites the reader is referred to the books by Smit and Wijn (3), Lax and Button (6), and Gurevich and Melkov (7); the articles by Gilleo and Nicholas, Chapters 1 and 4, respectively, in a handbook edited by Wohlfarth (8); and the article by Rodrigue (9).

Spinels. The chemical composition of spinel-ferrites is characterized by $MeFe_2O_4$, where Me represents one or more two-valent transition metals, such as Mg, Mn, Fe, Ni, Co, Cu, or Zn. Alternatively the two-valent metal can be replaced by a combination of a single-valent metal (such as Li) and a three-valent metal (such as Fe). The Fe shown in the generic formula is three-valent in a stoichiometric compound. These ions can also be replaced by other three-valent ions, such as Al and Ga. Figure 2 shows the spinel crystal structure and illustrates the various sites that can be occupied by the metal or oxygen ions. The metal ions are distributed over the a-sites, which are tetrahedrally surrounded by oxygen ions, and the b-sites, which are octahedrally surrounded by oxygen ions. The structure contains twice as many b-sites as a-sites. Thus, there is just enough room for all three-valent ions on b-sites and all two-valent ions on a-sites. Such a structure is called a normal spinel. By far most technically important ferrites are so-called inverse spinels, in which the three-valent ions occupy the a-sites and half of the b-sites, with two-valent ions on the remaining b-sites.

Studies of the saturation magnetization as a function of temperature have shown that, at low temperature, the magnetic moments of all ions on a-sites are aligned parallel to each other, as are the moments on all b-sites, but the two sets of moments are aligned anti-parallel. This implies that in spinel-ferrites without three-valent ion substitution the magnetic moments of the three valent Fe will cancel out, because half of it is on each type of site. Further information on this subject can be found in Ref. (3).

Garnets. The garnet-ferrites were discovered in 1956 by Bertaut and Forrat (10) and independently by Geller and Gilleo (11) in 1957. Their chemical composition can be characterized by $RE_3Fe_5O_{12}$. In this generic formula RE represents a rare-earth metal or a chemically similar metal, such as Yttrium (Y). A stoichiometric compound of this composition contains only three-valent metal ions. The Fe in this formula can be partially replaced by other three-valent metals, such as Al, Ga, Cr, or In, with a resultant lowering of the Curie temperature. Joint substitution of two- and four-valent metals (for instance Ca and V) is also possible and has resulted in technologically useful materials. Yttrium–iron garnet ($Y_3Fe_5O_{12}$), a material of special interest because of its exceptionally low dielectric and magnetic loss at microwave frequencies, is often referred to as YIG.

In the garnet lattice the metal ions are distributed over three types of sites: octahedral or a-sites (of which there are 16 in a unit cell of the crystal), tetrahedral or d-sites (24 per unit cell), and dodecahedral or c-sites (24 per unit cell). The ferric ions occupy the a and c sites and the RE or Y ions occupy the d-sites. The garnets are ferrimagnetic. If the RE ions are nonmagnetic (as in the case of Y^{3+}, La^{3+}, and Lu^{3+}) only the antiferromagnetically coupled a- and c-sublattices contribute to the net magnetic moment. If the RE ions are magnetic (as for instance in the case of Gd^{3+}) the d-sublattice is antiferromagnetically coupled to the normally dominant c-sublattice. Under these conditions the net magnetic moment of the material can go through zero at some intermediate temperature less than the Curie temperature. This temperature is known as the compensation temperature or compensation point. $Gd_3Fe_5O_{12}$ has a compensation point near room temperature. Winkler (12) has given a detailed review of the properties of magnetic garnets and of the techniques used for producing bulk and film materials.

Hexagonal Ferrites. Four different types of hexagonal ferrites, known as the M, W, Y, and Z types, have been studied. Their compositions are characterized as follows: M = $BaFe_{12}O_{19}$, W = $BaMe_2Fe_{16}O_{27}$, Y = $Ba_2Me_2Fe_{12}O_{22}$, Z = $Ba_3Me_2Fe_{24}O_{41}$. Here Me is a two-valent transition metal, and Ba can be replaced by Sr or Ca. The M-type hexaferrite is widely used as an inexpensive permanent magnet material, and has also been demonstrated as a useful material for nonreciprocal millimeter wave devices that require no external bias magnet (13,14). This material is often referred to as BaM. For a detailed review of hexagonal ferrites see Ref. (3).

Other Classifications: Film Deposition. Apart from their chemical composition, ferrite materials must also be characterized with regard to their crystallinity. Single-crystals have been grown of several of the technologically important compositions, such as $Y_3Fe_5O_{12}$ (YIG), $Li_{0.5}Fe_{2.5}O_4$, and $BaFe_{12}O_{19}$ (BaM), for instance. Single-crystals tend to be quite expensive and have therefore been used only in critical applications, where their narrow FMR line width is a decisive advantage over polycrystalline materials. Polycrystalline ferrites are used much more extensively, since they can be produced in a wide variety of compositions, are less expensive, and usually satisfy all the relevant device requirements.

Single-crystals as well as polycrystals can be produced by bulk processing and by thin-film deposition techniques. Ferrite films have many interesting applications in microwave technology, as discussed by Webb (15). Thin-film deposition usually results in polycrystalline films, but if the substrate is a single-crystal with a lattice spacing close to that of the deposited material, a single-crystal film can be obtained. An example is the deposition of $Y_3Fe_5O_{12}$ and similar magnetic gar-

nets on substrates of gadolinium–gallium garnet (GGG), a material that can readily be grown as a bulk single-crystal.

Arguably the most commonly used method for depositing thin films of ferrite materials is the liquid-phase epitaxi (LPE) method. This process involves immersing the substrate at high temperature into a melt of a suitable material (e.g. borates, in the case of garnets), in which the desired material to be deposited has been dissolved. By careful control of the temperature and the temperature gradients, and by suitable agitation of the melt, garnet films of a wide range of thicknesses (up to approx. 100 μm) have been grown by this method. For detailed information about the deposition of magnetic garnets by LPE, see Winkler (12). The LPE method has been less successful for spinel and hexagonal ferrites, primarily because an ideal substrate, such as GGG for magnetic garnet films has not yet been found. Truedson et al. (16) reported FMR measurements on BaM films deposited on single crystal substrates of $ZnGa_2O_4$. The narrow FMR line width (approx. 30 Oe = 24 A/cm), as well as x-ray data indicate that these BaM films are good-quality single-crystals.

Ferrite films can also be made by the pulsed laser deposition (PLD) method. In this process a polycrystalline ferrite plate of the desired composition is positioned opposite the substrate in a vacuum chamber and subjected to high-power pulsed laser irradiation. A suitable oxygen vapor pressure is maintained in the chamber to prevent oxygen loss during the deposition process. The PLD method has been used on several spinel, garnet, and hexagonal ferrites with considerable success (17–19). One of its attractive features is the possibility of depositing a ferrite film on a semiconductor substrate for integrated circuits (20). Stringent process control is required in this case, in order to prevent deterioration of the semiconductor due to exposure to high temperatures.

Two further ferrite deposition methods are the related spin spray process and the ferrite plating process (21,22). In these processes, an aqueous solution, containing the elements of the desired ferrite in the right proportions, is either sprayed on or flows over the substrate in a deposition cell at slightly elevated temperatures (approx. 90°C). Films of Fe_3O_4 and several ferrous ferrites have been grown successfully. The deposition process can be enhanced by ultrasonic excitation of the deposition cell (23). Ferrite films grown by the plating method are potentially of interest for microwave applications, because of the low deposition temperature. However, until now these films have generally shown excessive dielectric loss for such applications.

Fundamental Magnetic Properties of Microwave Ferrites

An important property of all ferromagnetic and ferrimagnetic materials is their crystalline anisotropy energy [see for instance Ref. (3) or (24)]. This concept is used to describe the tendency of the magnetization vector to become aligned with certain crystallographic directions, the so-called *easy* directions. The magnetic energy depends on the direction in which the material is magnetized. For materials with cubic symmetry (spinels and garnets), the easy directions are the cube edge directions ([100] or equivalent directions) or the body diagonal directions ([111] or equivalent directions), depending on the algebraic sign of the first-order cubic anisotropy constant K_1. If $K_1 < 0$, which is true for almost all of the technologically important materials, the easy directions are the [111] directions. For hexagonal materials, the hexagonal crystal axis can be either an easy or a hard direction, depending on the sign of the relevant uniaxial anisotropy constant K_u. If the hexagonal axis is a hard direction, the plane perpendicular to this axis is an easy plane, which implies that the magnetization vector tends to lie in this plane. An example of an easy axis material is $BaFe_{12}O_{19}$ (BaM); an example of an easy plane material is $Ba_2Zn_2Fe_{12}O_{22}$ (Zn_2Y).

The effect of crystalline anisotropy on FMR arises from its influence on the shape and depth of the energy minimum created through the joint influence of the dc bias field and crystalline anisotropy. For cubic ferrite and hexagonal easy-axis ferrites that are magnetized in an easy direction the effect of crystalline anisotropy on the FMR frequency is exactly the same as an additional magnetic field. This built-in magnetic field can be observed directly in single-crystals, but also has important consequences for polycrystals, since it strongly influences the FMR line width and the field dependence of the dc magnetization. For cubic ferrites the anisotropy field H_a is given by $2K_1/M_s$, if $K_1 > 0$, and by $-4K_1/3M_s$ if $K_1 < 0$. For hexagonal easy axis ferrites H_a is given by $2K_u/M_s$, where K_u is the uniaxial anisotropy constant. In Table 1 the composition, saturation magnetization M_s, remanence ratio M_r/M_s, anisotropy field H_a, g-factor, relative permittivity ϵ_r', and Curie temperature T_C are listed for several technologically important ferrites. In most cases the data pertain to room tem-

Table 1. Fundamental Properties of Microwave Ferrites

Material	Composition (approx.)	$\mu_0 M_s$ (mT)	M_r/M_s	$\mu_0 H_a$ (mT)	g-Factor	ϵ_r' (relative permitt.)	T_C (°C)	Ref.
YIG at 300 K	$Y_3Fe_5O_{12}$	175	0.7	6.3	2.005	15.0	280	15
YIG at 90 K	$Y_3Fe_5O_{12}$	236	0.7	18.7	2.002	NA	280	15
Temp.-stable garnet	$Gd_{1.7}Y_{1.2}Fe_5O_{12}$	80	0.6–0.8	NA	2.08	13	300	15
Narrow line width garnet	$Y_{1.4}Ca_{1.6}Fe_{3.7}V_{0.8}In_{0.5}O_{12}$	75	0.5–0.7	$\simeq$5.0	2.00	14	155	65[b]
Mn-ferrite	$MnFe_2C_3$	500	0.6–0.8	9.3	2.00	9.3	300	3,15
Ni-ferrite	$NiFe_2O_3$	320	0.6–0.8	34.7	2.2	12.8	585	3,15
Li-ferrite	$Li_5Fe_{2.5}O_3$	375	0.6–0.8	36.2	2.08	16.0	640	3,15
Unoriented BaM	$BaFe_{12}O_{19}$	420	0.5	1700	2.0	17	460	3,8
Oriented BaM	$BaFe_{12}O_{19}$	420	0.95	1700	2.0	22[a]	460	3,8[b]

[a] Measured parallel to hexagonal axis.
[b] Some data by private communication from H. J. Van Hook.

perature, but for some materials the data applicable at nitrogen temperature (90 K) are also included. A comprehensive review of the experimental data on microwave ferrites available in 1964 has been given by Von Aulock (25).

MICROWAVE BEHAVIOR OF FERRITES AT LOW POWER

In the discussion of electron spin resonance (see Fig. 1) the effect of damping on the spin precession was entirely neglected. In the present section damping will be taken into account phenomenologically, and expressions for the microwave permeability of ferrites in the presence of a dc bias field are derived. Also discussed are the concepts of dc and RF demagnetizing factors and the external permeability of small ellipsoidal samples.

Gyromagnetic Equation of Motion with Damping

The gyromagnetic equation of motion shown on Fig. 1 can be augmented by an additional term that describes the drift toward lower energy: in other words, toward parallel alignment of the magnetization vector with the magnetic field vector. It is plausible, but by no means necessary, that the approach to the equilibrium state could occur in such a way that the magnitude of the magnetization vector remains constant. An equation that describes this behavior was first proposed by Landau and Lifshitz (26) and is here shown in a slightly different notation:

$$d\boldsymbol{M}/dt = -\gamma'\mu_0\boldsymbol{M}\times\boldsymbol{H} - (\gamma'\mu_0\alpha/M_s)\boldsymbol{M}\times(\boldsymbol{M}\times\boldsymbol{H}) \qquad (2)$$

An alternative form of this equation was suggested by Gilbert (27):

$$d\boldsymbol{M}/dt = -\gamma\mu_0\boldsymbol{M}\times\boldsymbol{H} + (\alpha/M_s)\boldsymbol{M}\times(d\boldsymbol{M}/dt) \qquad (3)$$

Here α is a pure number, the Gilbert damping constant. The two equations are mathematically identical, provided that $\gamma' = \gamma/(1+\alpha^2)$, as can readily be shown, using well-known vector identities.

The spin precession illustrated in Fig. 1 is modified by the damping torque in such a way that the magnetization vector gradually spirals in toward the field direction, the rate depending on α. Multiplication of Eq. (3) by $\boldsymbol{H}$ yields the following interesting result

$$\boldsymbol{H}\cdot d\boldsymbol{M}/dt = (\alpha/\gamma M_s)(d\boldsymbol{M}/dt)^2 \qquad (4)$$

which shows that the rate at which the magnetic system looses energy is positive and proportional to the square of dM/dt. We remark parenthetically that the use of this phenomenological description of damping can be justified by a microscopic theory of relaxation processes, but only if α is allowed to be a function of magnetic field and frequency, as will be discussed in the section *Microscopic Theories of Damping.*

Permeability Tensor

Assume now that the magnetic field consists of a constant bias field $\boldsymbol{H}_0$, applied in the z-direction and of sufficient strength to magnetize the material to saturation, and a small RF field $\boldsymbol{h}$. The magnetization vector will then also have a large dc component, in the z-direction and of magnitude M_s, and small RF components in the x- and y-directions. Assume further that the RF field has a periodic time dependence proportional to $\exp(j\omega t)$. Under these conditions the x- and y-components of the Landau–Lifshitz–Gilbert equation, Eq. (3), can be written as

$$\begin{aligned} j\omega(m_x+\alpha m_y) &= -\omega_H m_y + \omega_M h_y \\ j\omega(m_y-\alpha m_x) &= \omega_H m_x - \omega_M h_x \\ \omega_H = \gamma\mu_0 H_0 \quad &\text{and} \quad \omega_M = \gamma\mu_0 M_s \end{aligned} \qquad (5)$$

The simplest way to solve these equations is to seek solutions for the circularly polarized components $m_\pm = m_x \pm m_y$ induced by a circularly polarized driving field $h_\pm = h_x \pm h_y$. One finds after a straightforward calculation that

$$m_\pm = \chi_\pm h_\pm \qquad (6)$$

where the susceptibilities for circular polarization are given by

$$\chi_\pm = \omega_M/(\omega_H + j\alpha\omega \mp \omega) \qquad (7)$$

and the relative permeabilities are given by $\mu_\pm = 1 + \chi_\pm$. In the xyz coordinate system the relationship between $\boldsymbol{b}$ and $\boldsymbol{h}$ can be expressed as $\boldsymbol{b} = \mu_0\boldsymbol{\mu}\boldsymbol{h}$, where μ_0 is the permeability of vacuum, and the relative permeability tensor is

$$\boldsymbol{\mu} = \begin{vmatrix} \mu & -j\kappa & 0 \\ j\kappa & \mu & 0 \\ 0 & 0 & 1 \end{vmatrix} \qquad (8)$$

with

$$\begin{aligned} \mu &= 1 + (\chi_+ + \chi_-)/2 = 1 + \omega_M(\omega_H + j\alpha\omega)/[(\omega_H + j\alpha\omega)^2 - \omega^2] \\ \kappa &= -(\chi_+ - \chi_-)/2 = -\omega_M\omega/[(\omega_H + j\alpha\omega)^2 - \omega^2] \end{aligned} \qquad (9)$$

In accordance with common practice κ is defined such as to be positive for $\omega_H < \omega$ and small loss. For the case of zero loss, these equations were first derived by Polder (28). The permeability tensor shown in Eq. (8) is therefore known as the Polder tensor.

In the discussions and calculations presented in this section, we have disregarded the fact that the magnetic structure of ferrites is characterized by the existence of two oppositely polarized sublattices. This is usually a valid approximation, but in the vicinity of a magnetic compensation point the existence of the sublattice structure must be taken into account, since it leads to the possibility of an additional resonance, the *exchange resonance,* and to unusually large or small g-factors. Details on this subject may be found in Foner's review article, "Antiferromagnetic and Ferrimagnetic Resonance" (29).

Demagnetizing Factors and External Permeability

The susceptibilities given by Eqs. (6) and (7) relate the RF magnetization to the RF magnetic field existing inside the ferrite material; the dc bias field is similarly the bias field in the interior of the sample (possibly augmented by the built-in anisotropy field, as discussed previously). In this context, it is

important to remember that the internal magnetic field can differ substantially from the external field present at the site of the sample before the sample was inserted into the field. The field generated by the magnetic poles at the sample surface (the divergence of the magnetization vector) is usually referred to as the *demagnetizing field.* For samples of ellipsoidal shape, the demagnetizing field of a uniformly magnetized sample is itself uniform. It can be characterized by a tensor of demagnetizing factors. This tensor has diagonal form in a coordinate system aligned with the principal axes of the ellipsoid. The sum of the diagonal elements of the tensor always equals unity. This implies that for a sphere the demagnetizing factors equal 1/3 for all directions. For a very elongated circular cylinder (the limiting case of a prolate spheroid) the axial or longitudinal demagnetizing factor N_ℓ equals 0, and the transverse demagnetizing factors N_t equal 0.5. Similarly, for a very squat circular cylinder (the limiting case of an oblate spheroid), N_ℓ equals 1 and N_t equals zero.

For all applications that involve small samples of ferrite of near-ellipsoidal shape (for instance, microwave measurements on small spherical samples, or microwave filters using sphere resonators) it is useful to express the RF magnetization in terms of the external, rather than the internal magnetic field. The internal magnetic field is generally related to the external field by

$$\boldsymbol{h}_{\text{int}} = \boldsymbol{h}_{\text{ext}} - \boldsymbol{N}\boldsymbol{m} \tag{10}$$

where $\boldsymbol{N}$ is the appropriate demagnetizing factor. By using Eqs. (10) and (6) we can express the RF magnetization as a function of the external RF magnetic field, assuming an axially magnetized spheroid and circular polarization of the RF field. The result is

$$m = \chi_{\text{ext}} h \tag{11}$$

where the external susceptibility is related to the true (internal) susceptibility χ for both senses of circular polarization by

$$\chi_{\text{ext}} = \chi/(1 + N_t\chi) \tag{12}$$

For positive circular polarization in the case of zero loss one obtains, for instance

$$\chi_{\text{ext}} = \omega_M/(\omega_H + N_t\omega_M - \omega) \tag{13}$$

The external permeability tensor can now be obtained in a manner analogous to Eq. (8). The small-sample resonance frequency (frequency at which χ_{ext} is singular in the absence of loss) is according to Eq. (13) given by

$$\omega_{\text{res}} = \omega_H + N_t\omega_M = \gamma\mu_0 H_{\text{ext}} + (N_t - N_\ell)\omega_M \tag{14}$$

Here H_{ext} is the external dc bias field. Eq. (14) implies that for spherical sample shape the resonance frequency is proportional to the external bias field, since the dc and RF demagnetizing effects cancel.

Spin Waves

For a realistic description of ferro- and ferrimagnetic materials the gyromagnetic equations of motion in the form shown in Fig. 1 and Eqs. (2) and (3) must be modified to take account of the interaction that tends to keep the magnetic moments on adjacent sites in the lattice aligned parallel or anti-parallel. This interaction has a quantum-mechanical origin and is known as the *exchange interaction.* For the analysis and prediction of microwave properties of ferrites, the detailed atomic structure of the ferrite crystals rarely matters, and the magnetization vector can be regarded to be a continuous function of the spatial coordinates. In this approximation, the density of exchange energy is represented by a term that involves squares of the spatial first derivatives of the magnetization vector. In the linearized equations of motion, Eq. (5), the exchange energy leads to additional terms, and the appropriate equations are now

$$\begin{aligned} j\omega(m_x + \alpha m_y) &= -(\omega_H - D\nabla^2)m_y + \omega_M h_y \\ j\omega(m_y - \alpha m_x) &= (\omega_H - D\nabla^2)m_x - \omega_M h_x \end{aligned} \tag{15}$$

Here ∇^2 is the Laplace differential operator (the sum of the three second derivatives with respect to x, y, and z, or an equivalent form), and D is a numerical parameter that characterizes the strength of the exchange interaction.

In Eq. (15) the RF magnetic field $\boldsymbol{h}$ is the sum of an externally applied drive field (if any) and the RF field generated by the magnetization itself. The latter is usually called the dipolar field $\boldsymbol{h}_{\text{dip}}$. For the present purpose, it is sufficient to calculate it in the quasi-static approximation, where it is given by the conditions

$$\begin{aligned} \nabla \times \boldsymbol{h}_{\text{dip}} &= 0 \\ \nabla \cdot \boldsymbol{h}_{\text{dip}} &= -\nabla \cdot \boldsymbol{m} \end{aligned} \tag{16}$$

which determine $\boldsymbol{h}_{\text{dip}}$ uniquely. The approximation in Eq. (16) consists in neglecting the displacement currents in Maxwell's equations. This is approximately valid when the phase velocity of the spin wave is much smaller than the velocity of light, which is true in the present case.

Assume now that the RF magnetization varies sinusoidally with the spatial coordinates.

$$\boldsymbol{m}(\boldsymbol{r}) = \boldsymbol{m}_0 \exp(-j\boldsymbol{k} \cdot \boldsymbol{r}) \tag{17}$$

where $\boldsymbol{k}$ is the wave number vector. The dipolar field associated with this distribution of magnetization is readily shown to be

$$\boldsymbol{h}_{\text{dip}}(\boldsymbol{r}) = -(\boldsymbol{k} \cdot \boldsymbol{m}_0/k^2)\boldsymbol{k} \exp(-j\boldsymbol{k} \cdot \boldsymbol{r}) \tag{18}$$

In order to verify that Eq. (18) is correct, it may readily be shown that the expression for $\boldsymbol{h}_{\text{dip}}$ satisfies both parts of Eq. (16). Consider now a wave propagating at an angle θ to the direction of the dc bias field. Without loss of generality we may assume that its propagation vector $\boldsymbol{k}$ lies in the x–z plane:

$$\boldsymbol{k} = k \begin{vmatrix} \sin\theta \\ 0 \\ \cos\theta \end{vmatrix} \tag{19}$$

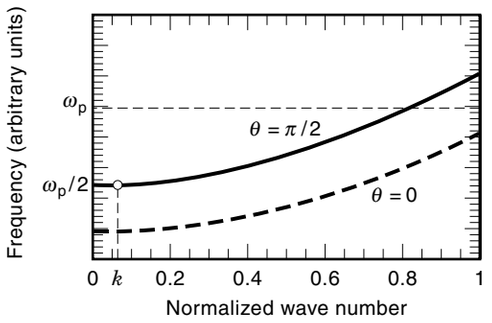

Figure 3. Spin-wave dispersion diagram, parallel pumping.

Combining Eq. (15) with (17) to (19), and taking the limit of zero loss one finds that the stipulated trial function satisfies all requirements, provided that

$$\begin{aligned} j\omega m_{0x} &= -(\omega_H + Dk^2)m_{0y} \\ j\omega m_{0y} &= (\omega_H + Dk^2 + \omega_M \sin^2\theta)m_{0x} \end{aligned} \tag{20}$$

The frequency of the spin waves is determined by the condition that the secular determinant vanishes, and is therefore given by

$$\omega_k = [(\omega_H + Dk^2)(\omega_H + Dk^2 + \omega_M \sin^2\theta)]^{1/2} \tag{21}$$

The spin precession associated with the spin wave is generally elliptical, becoming circular only in the limit $\theta \to 0$. The ratio of the magnetizations in the y- and x-directions is

$$|m_{0y}/m_{0x}| = [1 + \omega_M \sin^2\theta/(\omega_H + Dk^2)]^{1/2} \tag{22}$$

as can readily be verified from Eqs. (20) and (21). Figure 3 is a dispersion diagram for spin waves, showing frequency versus wave number for given θ.

MICROWAVE BEHAVIOR OF FERRITES AT HIGH POWER

The equations and discussions of the preceding chapter were based on the assumption that the ferrite material responds linearly to any RF magnetic field incident upon it, as appropriate at low power levels. It was discovered in the early 1950s, however, that ferrites have unexpectedly high loss at elevated power levels (30–32), and that this loss often sets in at a well-defined threshold. These observations were explained by Suhl (33) who pointed out that the nonlinear effects could be attributed to the "parametric excitation" of spin waves. He showed that the excitation of the uniform precessional mode, which may be considered to be a spin wave with wave number zero, produces a time-varying coupling between pairs of spin waves traveling in opposite directions. Under the influence of this time-varying coupling, the motion of the spin waves becomes unstable, as soon as the amplitude of the uniform mode exceeds a certain threshold. Beyond the threshold, the spin waves are excited to a level much higher than that corresponding to thermal equilibrium. For a detailed description of Suhl's theory and a general review of FMR at high power levels, see Damon (34).

The parametric excitation of spin waves first discussed by Suhl (33), which occurs with an RF field applied perpendicular to the dc bias field, is a rather complicated phenomenon. A simpler situation occurs, when the RF field is applied parallel to the dc bias field. Schloemann and collaborators (35–37) showed that parametric excitation of spin waves occurs also under these conditions, and that this effect can conveniently be used in the study of relaxation processes in ferrites. The parametric excitation process responsible for spin-wave instability is qualitatively illustrated in Fig. 4. If the spin precession is circular, as shown on the left, an RF field applied parallel to the dc bias field only speeds up and slows down the rate of precession without affecting the cone angle. With elliptical spin precession, shown in the middle, the situation is analogous to that of an ideal pendulum that is periodically moved up and down, as shown on the right. Although such an up-and-down motion cannot excite the pendulum from its (lowest energy) rest position, it can amplify any existing vi-

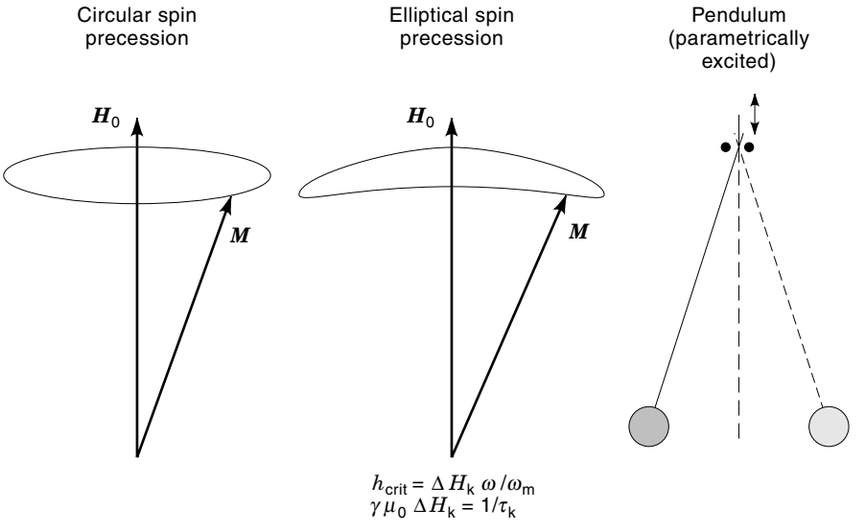

Figure 4. FMR and parametric excitation of spin waves by parallel pumping.

bration; and the same is true for elliptical spin precession. Instability sets in at the critical RF field strength shown at the bottom of Fig. 4, as discussed subsequently. In the present section the parametric excitation by parallel pumping is first discussed using as little mathematical analysis as possible, and then more rigorously in calculations of the instability threshold, the subthreshold behavior, and transient effects above threshold. The section concludes with a discussion of spin wave instability under perpendicular pumping.

Parametric Excitation of Spin Waves by Parallel Pumping

It was shown in the section entitled *Spin Waves* that for spin waves the spin precession generally follows an elliptical path, the ellipticity being largest for waves traveling perpendicular to the dc bias field direction. Figure 5 shows the elliptical path of the tip of the magnetization vector. Since the length of this vector remains constant, the z component must vary at twice the precession frequency. Consider now the influence of an RF magnetic field $h_z(t)$ applied parallel to the dc bias field. Let the frequency of this pump field equal twice the precession frequency and assume the precessional motion is already established before the pump field is switched on. For investigating the effect of the pump field on the spin precession motion, the phase relation between this motion and the pump field is important.

Consider the case in which this phase relation is such that the pump field adds to the dc field at points 1 and 3 of the precession cycle and subtracts at points 2 and 4, as indicated in Fig. 5. The resultant contributions to the rate of change of the RF magnetization are shown as $\delta\, d\boldsymbol{m}/dt$ in Fig. 5. Note that the arrows point to the exterior of the precession ellipse in each case. This implies that the pump field tends to increase the precession angle if the assumed phase relation is in fact realized. This tendency is at least partially compensated by relaxation processes, which always tend to decrease the precession angle. Instability occurs when the pump field is sufficiently large to overcome the relaxation processes. If the phase of the pump field is reversed, all the $\delta\, d\boldsymbol{m}/dt$ arrows in Fig. 5 would point to the interior of the ellipse, indicating that instability does not occur under these conditions.

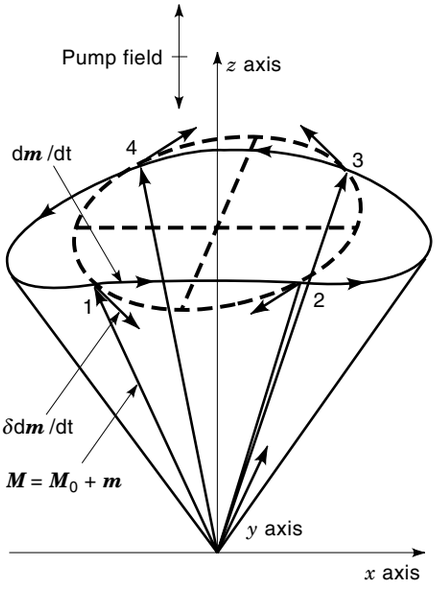

Figure 5. Physical explanation of spin-wave instability in an RF magnetic field applied parallel to the dc field.

For the mathematical analysis of spin-wave instability, the linearized equations (analogous to Eq. (15), but with an unspecified time dependence) can serve as the starting point, but the presence of the time-varying field in the z-direction must be taken into account. Spatially periodic boundary conditions are imposed on the transverse magnetization, and the equations of motion for the Fourier components of the transverse magnetization are determined. For convenience these equations are formulated in terms of complex variables $m(r) = m_x + jm_y$. Simple equations are obtained for the Fourier components of $m(r)$, denoted as m_k, where k is the wave number. In the absence of a pump field, these variables are close to being normal modes of the problem, since the equations are almost decoupled. However, the rate of change of m_k depends not only on m_k but also on m^*_{-k}, where the asterisk denotes the complex conjugate. A linear transformation between the Fourier components m_k and m^*_{-k} and new variables a_k and a^*_{-k} is required to decouple the equations completely, as first pointed out by Holstein and Primakof (38). These variables can be interpreted as the spin wave amplitudes, since the energy of each spin wave is proportional to $a^*_k a_k$. In terms of these variables, the equations of motion in the presence of a pump field $h_z = h_{z0}\cos(\omega t)$ can be shown to be

$$a^*_k = j(\Omega_k a_k - c_k \cos(\omega t) a^*_{-k}) \tag{23}$$

Here

$$\Omega_k = \omega_k + j\eta_k \tag{24}$$

$$c_k = \gamma\mu_0 h_{z0}(\omega_M/\omega_k)\sin^2\theta_k \exp(2j\phi_k) \tag{25}$$

dissipation has been taken into account by assigning a positive imaginary part to the resonance frequency, θ_k and ϕ_k are the polar and azimuth angles of the wave number vector, and a time-varying term proportional to a_k has been neglected, because it does not contribute to spin-wave instability.

In order to solve Eq. (23) consider the trial solution

$$a_k \propto \exp[(\tfrac{1}{2}j\omega + \kappa)t] \tag{26}$$

where κ is an unspecified rise constant, which will be chosen in such a way that the trial solution is an approximate solution of Eq. (23). By inserting Eq. (26) into Eq. (23) and neglecting off-resonance components, one obtains

$$[\omega_k - \tfrac{1}{2}\omega + j(\eta_k + \kappa)]a_k = \tfrac{1}{2}c_k a^*_{-k} \tag{27}$$

The rise constant is now determined from the condition that this equation and its adjoint (the complex conjugate equation with k replaced by $-k$) are simultaneously satisfied, with the result

$$\kappa = -\eta_k \pm [\tfrac{1}{4}|c_k|^2 - (\omega_k - \tfrac{1}{2}\omega)^2]^{1/2} \tag{28}$$

Equation (28) shows that instability (positive κ) occurs most readily when the spin-wave frequency equals half the pump frequency, and requires a pump field h_{z0} that is larger than a

certain critical field h_{crit}. By using Eq. (25), h_{crit} is determined to be

$$h_{\text{crit}} = (\omega/\omega_M) min(\Delta H_k / \sin^2 \theta_k) \tag{29}$$

Here, $\Delta H_k = 2\eta_k/\gamma\mu_0$ is the spin-wave line width, and the minimum must be taken with respect to the wave number k subject to the condition $\omega_k = \frac{1}{2}\omega$.

By referring to Fig. 3 the reader can easily see that instability will occur at a finite wave number and $\theta = \pi/2$ when the bias field is less than a certain characteristic value

$$H_c = -\tfrac{1}{2}M_s + [(\tfrac{1}{2}M_s)^2 + (\omega/2\gamma\mu_0)^2]^{1/2} \tag{30}$$

On the other hand, the instability will occur at some very small wave number and a suitable value of θ between zero and $\pi/2$, when the bias field is between H_c and $\omega/2\gamma\mu_0$. The instability is inhibited when the bias field is larger than $\omega/2\gamma\mu_0$.

The theoretical analysis summarized in Eqs. (23)–(28) can also be used for predicting other high-power effects that are related to spin-wave instability. It can be shown, for instance, that for $h_{z0} < h_{\text{crit}}$ the parametric excitation gives rise to a sub-threshold steady-state absorption, and that this steady-state absorption diverges as the threshold is approached. Similarly, the transient growth of the spin-wave population immediately above the threshold can be analyzed, and quantitative predictions can be derived (39,40). For this purpose the equations summarized here must be augmented by a thermal drive field, a stochastic function of time, defined in such a way that the squares of the spin-wave amplitudes asymptotically approach the thermal equilibrium values, regardless of the initial conditions (40,41). The absorption coefficient for the steady-state absorption, calculated in this way, approaches a finite limit as the RF field amplitude is reduced to zero. The value obtained in this way agrees with that obtained by Kaganov and Tsukernik (42), using a different approach valid only for low power levels. The experimental observation of this effect was reported by Hartwig et al. (43). Measurements of the dc moment induced by a strong RF field applied parallel to the dc field confirmed the theoretical predictions concerning this aspect of parallel pumping (44).

Parametric Excitation of Spin Waves by Perpendicular Pumping

Nonlinear effects in magnetic materials were first observed in the conventional configuration of ferromagnetic resonance experiments with the RF magnetic field applied perpendicular to the dc bias field. The early observations of Bloembergen, Damon, and Wang (30–32) were later interpreted by Suhl (33), who showed that the observed phenomena could be attributed to parametric excitation of spin waves.

The physical processes that lead to spin-wave instability under perpendicular pumping are very similar to those that produce instability under parallel pumping. For perpendicular excitation the RF field primarily excites the uniform mode of the sample. The uniform mode, in turn, induces a time-varying coupling between spin waves propagating in opposite directions and hence gives rise to parametric excitation of these waves. Parametric processes of first and second order must be distinguished. For the first-order process, the time-varying coupling is proportional to the first power of the uniform mode amplitude: that is, to the precession angle. Spin waves that resonate at half the pump frequency are most susceptible to instability due to this process. The second-order process is induced by a time-varying coupling that is proportional to the square of the uniform mode amplitude. The spin waves that are most susceptible to instability due to this process resonate at the pump frequency.

For a given RF field strength the amplitude of the uniform mode is largest when the sample is biased to resonance. The lowest threshold for instability, therefore, occurs at resonance, provided that the first-order process is allowed under these conditions. For a spheroidal sample with a transverse demagnetizing factor N_t the resonant frequency of the uniform mode is given by Eq. (14). The lowest spin wave frequency, on the other hand, is given by ω_H [see Eq. (5)]. First-order instability can occur at resonance if

$$2\omega_H \leq \omega_{\text{res}} \tag{31}$$

By eliminating ω_H between Eqs. (31) and (14) this condition can alternatively be expressed as

$$\omega_{\text{res}} \leq \omega_c \quad \text{and} \quad \omega_c \equiv 2\omega_M N_t \tag{32}$$

For spherical samples ($N_t = \frac{1}{3}$) of YIG at room temperature ($\mu_0 M_s = 175$ mT) the first-order process is allowed at resonance when the pump frequencies is below 3.3 GHz.

If the first-order process is not allowed at resonance, spin wave instability will occur by virtue of the second-order process. The instability threshold for this process is usually much higher than for the first-order process. When the strength of the dc bias field is reduced below resonance, the first-order process becomes allowed, because spin waves that resonate at half the pump frequency now become available. If the experimental conditions (in regard to frequency, saturation magnetization, and sample shape) are such that the inequality in Eq. (32) is violated, second-order instability is observed at resonance and first-order instability occurs at dc bias fields sufficiently below resonance. The first-order instability is manifested as a subsidiary absorption peak, which occurs at bias fields below resonance. The height of the main resonance absorption peak is reduced by the second-order spin-wave instability. When the first-order instability is allowed at resonance, the subsidiary absorption peak is said to coincide with the main resonance. The inequality Eq. (32) is, therefore, also known as the coincidence condition.

We now summarize briefly the theoretical expressions for the critical field derived from Suhl's theory (33). These formulas are primarily applicable to axially magnetized spheroidal samples, which are excited by a circularly polarized RF magnetic field. The critical RF field as given in these formulas is the amplitude of the circularly polarized RF field. In the experimental practice, a linearly polarized driving field is used in most cases. Under these conditions the formulas given subsequently are still applicable to a good approximation. The linearly polarized field can be decomposed into two circularly polarized fields, which have opposite senses of rotation. The negative circular component is practically ineffective, because it does not excite the resonance. Thus, the given formulas are approximately correct for the case of a linearly polarized driving field, if the right hand sides are multiplied by two.

When the first-order process is allowed at resonance the critical field is

$$h_{\text{crit}} = (\Delta H \Delta H_k / M_s) F(\omega, \omega_M, \omega_c) \tag{33}$$

where ΔH is the line width (of the uniform mode), ΔH_k is the spin wave line width as defined in connection with Eq. (29), and F is a numerical factor that is usually of order unity, but becomes very large when the first-order process becomes forbidden. Expressed in terms of the characteristic frequency ω_c of Eq. (32), F is given by

$$F(\omega, \omega_M, \omega_c) = \frac{2\omega\omega_M(2\omega - \omega_c)}{(\omega_c - \omega)^{1/2}(3\omega - \omega_c)^{3/2}[3\omega^2 + 4\omega(\omega_M - \omega_c) - (2\omega_M - \omega_c)\omega_c]^{1/2}} \tag{34}$$

provided that $\omega_c - \omega$ is positive but not too large. The range of validity of Eq. (34) depends on the shape of the sample.

The critical field for second-order instability is given by

$$h_{\text{crit}} = 0.5\Delta H(\Delta H_k / M_s)^{1/2} \tag{35}$$

The spin waves that are most susceptible to second-order instability propagate in the direction of the dc field; those most susceptible to first-order instability propagate under an angle of approximately 45° to this direction.

In the calculations of the instability threshold summarized in Eqs. (34) and (35), the effect of crystalline anisotropy has been neglected. The anisotropy leads to substantial corrections when the anisotropy field is comparable with M_s for both parallel and perpendicular pumping. For perpendicular pumping the major effect of crystalline anisotropy is to modify the coincidence condition. For instance, in materials with large easy-plane anisotropy that are magnetized in the easy plane, the characteristic frequency ω_c, below which the first-order process can occur at resonance, is substantially higher than the value given in Eq. (32). For details see the original literature (45).

MICROSCOPIC THEORIES OF DAMPING

For many ferrite microwave devices the insertion loss is an important performance parameter. Since the insertion loss is often largely determined by the damping processes that are associated with FMR, much effort has been devoted to developing ferrite materials with low loss and narrow FMR line width. To facilitate this search for better materials, an adequate theoretical understanding of the relaxation processes that occur in ferrites and other magnetic materials is essential. The phenomenological description of damping, introduced previously, is useful but does not actually provide an explanation of the observed physical effects. In this section we review various microscopic theories that have been proposed to explain the damping effects observed in ferrites, and will compare the theories with experimental data, where appropriate.

Dissipation processes in ferromagnetic materials have been studied and investigated by many authors. For detailed background information, see Refs. 46–50.

Overview of Damping Processes in Ferrites

The basic physical problem to be considered is as follows: A ferro- or ferrimagnetic material, initially in thermal equilibrium at some given temperature, is excited by an external signal, such as an RF magnetic field. We assume for simplicity that the signal excites only a single degree of freedom, such as the uniform mode of a small ellipsoidal sample of ferrite. The energy transferred to this particular mode from the signal will gradually be distributed to other degrees of freedom of the sample, and will ultimately become distributed over all degrees of freedom as heat energy.

This scenario is illustrated in Fig. 6, which shows the most important relaxation mechanisms that occur in ferrites. A single mode (for instance the uniform mode in FMR) or a small group of modes (for instance a group of spin waves in parallel pumping) are excited by an electromagnetic signal. The excited modes can distribute their energy within the magnetic system (symbolically represented by the large square on the left) or by interaction with other degrees of freedom (charge carriers, lattice vibrations, strongly relaxing ions, etc.). In low-loss microwave ferrites, the interactions within the magnetic system appear to be the most important. We will therefore focus attention on these relaxation processes.

The general procedure for calculating relaxation rates begins with the determination of the normal modes of the system (spin waves, lattice vibrations, etc.). Next, the energy is expressed in terms of the normal mode amplitudes. This expression then becomes the Hamiltonian of the system. The linear term of this Hamiltonian vanishes, because the normal mode amplitudes are defined as deviations from the energy minimum. The second-order term of the Hamiltonian (H_2) describes noninteracting normal modes. Higher order terms, summarized in H_w, describe the interactions between the normal modes.

$$H = H_0 + H_2 + H_w \tag{36}$$

In quantum mechanics the normal mode amplitudes can be interpreted as creation and annihilation operators that obey the commutation rule

$$a_k a_{k'}^* - a_{k'}^* a_k = \delta_{k-k'} \tag{37}$$

In terms of these operators, the second order Hamiltonian H_2 becomes

$$H_2 = \hbar \sum_k \omega_k a_k^* a_k \tag{38}$$

where $a_k^* a_k = n_k$ is the occupation number of mode k. The eigen states of the Hamiltonian H_2 are characterized by a set of integer occupation numbers n_k. Because of dipolar and exchange interactions, H_w contains terms like

$$\begin{aligned} &\Phi_{kk'k''} a_k a_{k'} a_{-k''}^* + c.c. \\ &\Phi_{kk'k''k'''} a_k a_{k'} a_{-k''}^* a_{-k'''}^* + c.c. \end{aligned} \tag{39}$$

which induce transitions between these eigenstates. The probability, per unit time, of a transition induced by such terms between an initial state i and a final state f, can be

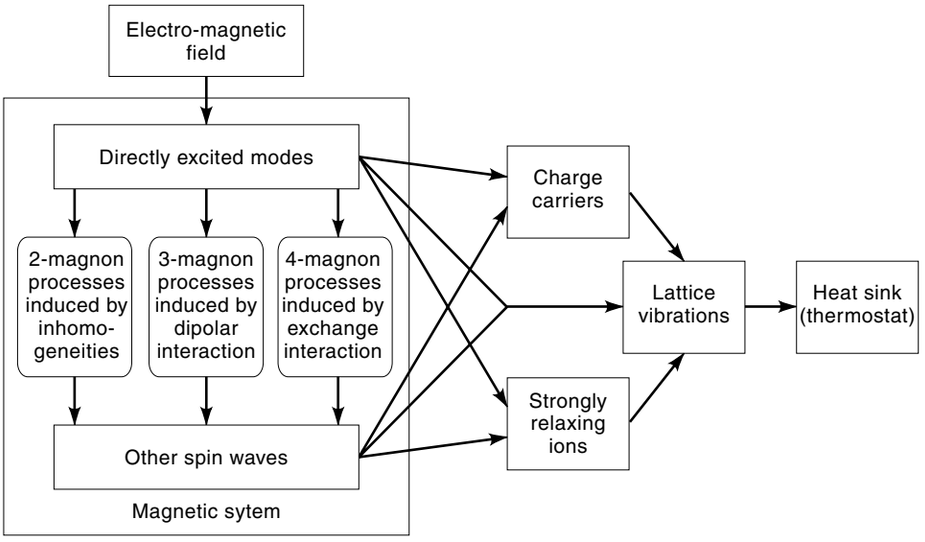

Figure 6. Energy flow in FMR and spin-wave instability.

calculated by time-dependent perturbation theory, with the result

$$\lambda_{if} = \frac{2\pi}{\hbar} |H_w|_{if}^2 \, \delta(E_i - E_f) \tag{40}$$

The rate of change of the mean occupation number $\overline{n}_k$ of mode k can then be calculated. If only k is excited above thermal equilibrium, the resulting equation is of the form

$$d\overline{n}_k/dt = -2\eta_k(\overline{n}_k - \langle n_k \rangle) \tag{41}$$

where $\langle n_k \rangle$ is the thermal equilibrium value of n_k and $2\eta_k$ is the relaxation rate.

As indicated in Fig. 6, the third- and fourth-order terms of the Hamiltonian induce relaxation processes, which are usually labeled as 3-magnon and 4-magnon processes (a magnon being a quantum of spin-wave energy). These processes occur in all ferro- and ferrimagnetic materials, in particular in perfect single crystals of ultrapure low-loss materials, such as YIG, and are therefore properly called intrinsic. Additional, nonintrinsic relaxation processes are important in materials that contain imperfections, such as crystal defects, nonmagnetic inclusions (including pores), and grain boundaries (for polycrystals). Imperfections and inhomogeneities of this type can be described by an additional second-order term in the Hamiltonian, an interaction between spin waves of different wave number. The relaxation processes induced by this interaction are usually referred to as 2-magnon processes.

Intrinsic Damping Processes in Ideal Materials

As first pointed out by Akhiezer (51), the dipolar energy contains contributions of third order in the spin-wave amplitudes. The exchange energy, on the other hand, does not contain any contributions of that order, but it does contain contributions of fourth order. Akhiezer (51) and many authors after him (52–56) have contributed significantly to the theory of intrinsic relaxation processes induced by these higher order terms in the Hamiltonian.

The third-order Hamiltonian induces transitions, in which one magnon is absorbed and two are emitted (splitting process) or two magnons are absorbed and one is emitted (confluence process). In these transitions Zeeman energy is converted into dipolar and exchange energy, and vice versa. In Fig. 7, the 3-magnon splitting and confluence processes are illustrated by simple diagrams. In the splitting process, the directly excited magnon (k) splits into two magnons k' and k'', under conservation of energy and momentum. Analysis shows that the conservation laws can be satisfied in two different ways, giving rise to two kinds of splitting processes: the low-k process (allowed only for frequencies less than $(2/3)\omega_M$, see Ref. (54)), and the high-k splitting process (allowed only for sufficiently high k, which implies high frequency, see Ref. 57). Both of these processes give a contribution to the relaxation rate of spin waves that remains finite as the wave number approaches zero. The 3-magnon confluence process, on the other hand, gives a contribution to the relaxation rate that is proportional to k (for small k), at least for ferromagnetic materials. It has been proposed, however, that in ferrimagnetic materials an analogous process involving the exchange branch of the spin-wave spectrum can give a k-independent contribution to the relaxation rate (58).

In the 4-magnon scattering process, also illustrated in Fig. 7, a directly excited magnon k combines with a thermal magnon k' and forms magnons k'' and k''', under conservation of energy and momentum. It has been shown (55) that the relaxation rate induced by this process is proportional to k^2. It might be expected that the 4-magnon process, being of higher order than the 3-magnon process, would always give a smaller contribution to the relaxation rate. This is not necessarily true, however, because the exchange interaction is fundamentally a much stronger interaction than the dipolar interaction.

As mentioned in the previous section, the observation of spin-wave instability under parallel pumping, provides an opportunity to study relaxation phenomena by experiments, in particular the k-dependence of the relaxation rate. The validity of the theoretical predictions described can thus be determined. Figure 8 summarizes the results of measurements of the spin-wave line width ΔH_k as a function of wave number, using a spherical sample of high-purity YIG at a pump fre-

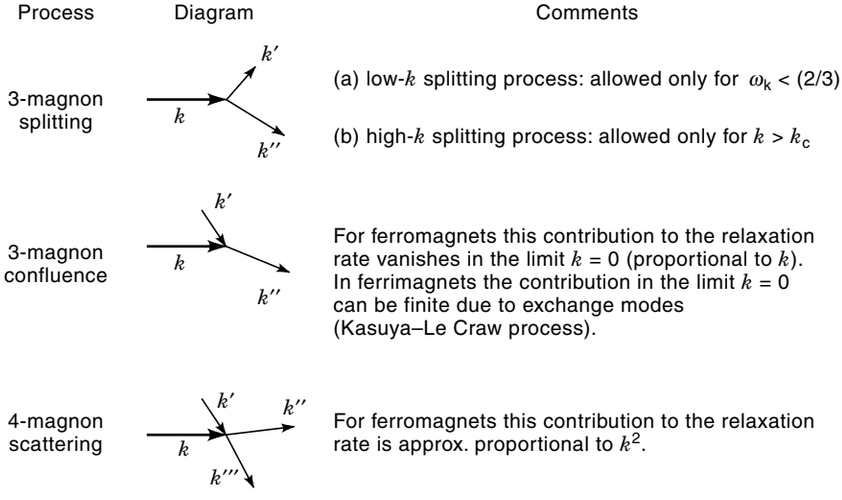

Figure 7. Inherent spin-spin relaxation processes.

quency of 35.5 GHz (7). The points represent the data obtained at room temperature. The labels on the various lines representing theoretical calculations are explained in the inset. In comparing their experimental results with the various theories mentioned in connection with Fig. 7, the authors assumed a theoretical k-independent contribution of approximately 0.28 Oe (labeled $\Delta H_{k\to 0}$ in Fig. 8), which is not the result of a quantitative theoretical calculation. All other curves are deduced straightforwardly from bona fide theories.

Nonintrinsic Damping Processes

Two important classes of nonintrinsic damping processes should be distinguished. The first class comprises processes induced by fast-relaxing ions, such as rare-earth ions (other than Gd^{+++}), Co^{++}, and ferrous iron Fe^{++}. If these ions are present within the spinel or garnet lattice, the FMR line width is increased significantly, particularly at cryogenic temperatures. These relaxation processes are discussed in detail in Refs. (48) and (49). The second class comprises processes induced by inhomogeneity of the ferrite material. The most important example of this type of process is the spin-wave scattering induced by polycrystallinity in combination with local crystalline anisotropy (59). In the present subsection we will primarily focus on this contribution to the relaxation rate.

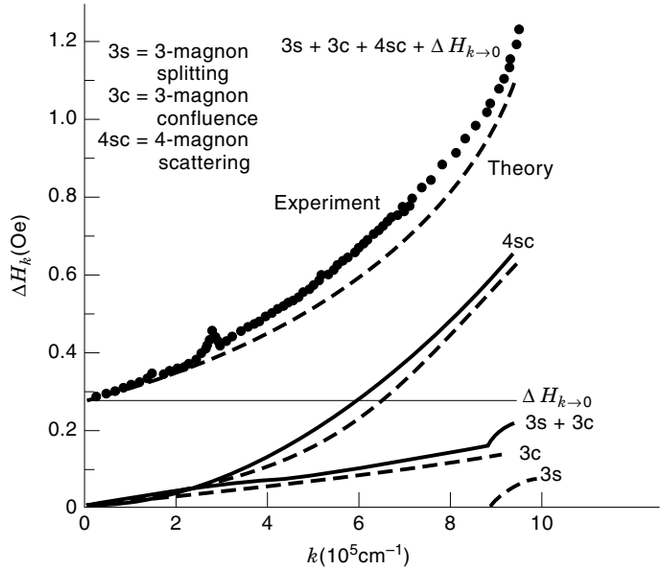

Figure 8. Contributions of different relaxation processes to the damping of spin waves in YIG. [After Gurevich and Melkov (7).]

In the spin-wave Hamiltonian introduced in Eq. (36), a locally varying anisotropy field gives rise to an interaction Hamiltonian of the form

$$H_w = \hbar \sum_{kk'} P_{kk'} a_k^* a_{k'} \tag{42}$$

where the coefficients $P_{kk'}$ are proportional to the Fourier transform $H(k - k')$ of the local anisotropy field. By applying time-dependent quantum-mechanical perturbation theory in the manner outlined in the previous section, one can show that the relaxation time of the uniform mode is given by

$$1/\tau_0 = 2\pi \sum_k |P_{0k}|^2 \delta(\omega_k - \omega_0) \tag{43}$$

in this case. Here ω_k and ω_0 are the resonant frequencies of spin-waves and of the uniform mode, respectively. Since this expression is independent of the signal frequency ω, it might be interpreted as implying that the FMR line width has a Lorentzian shape, but such a conclusion is not justified, as we will show presently.

The inhomogeneity induced spin-wave scattering can also be analyzed by an equations-of-motion approach, which happens to be simpler in this case than the standard approach outlined previously. By calculating the susceptibility for positive circular polarization, one obtains (59)

$$\chi_+ = \omega_M \Big/ \left[\Omega_0 - \omega - \sum_k |P_{0k}|^2 / (\Omega_k - \omega) \right] \tag{44}$$

where terms of higher order in the perturbation have been neglected in the denominator, and Ω_0 and Ω_k are complex resonance frequencies ($\Omega_k = \omega_k + j\eta_k$). In the limit of very small

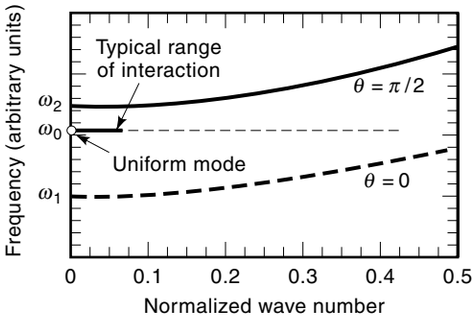

Figure 9. Two-magnon interaction induced by a long-wavelength inhomogeneity. Line width is dependent on frequency and internal magnetic field. Line shape is nonLorentzian.

intrinsic damping, the result shown in Eq. (44) is very similar to Eq. (43), since the effective relaxation rate (imaginary part of the denominator in Eq. (44)) can then be expressed (59) as

$$\eta_{0\text{eff}} = \eta_0 + \pi \sum_k |P_{0k}|^2 \delta(\omega_k - \omega) \tag{45}$$

For $\omega = \omega_0$, Eqs. (45) and (43) agree completely, since

$$1/\tau_0 = 2\eta_{0\text{eff}} \tag{46}$$

The equations-of-motion approach makes it clear that the effective relaxation rate is dependent on the signal frequency, a fact that the standard approach (quantum-mechanical perturbation theory) tends to obscure. In the presence of inhomogeneity induced scattering the FMR line shape is decidedly nonLorentzian, because the effective relaxation rate is strongly dependent on the signal frequency.

This may be understood intuitively with the help of Fig. 9, which shows the usual spin-wave band and the resonant frequency of the uniform mode inside the spin-wave band. The local anisotropy field has significantly large Fourier components only for relative small wave numbers (approximately up to the inverse of the average grain size). Thus, the range of interaction in k-space is limited to some relatively small region, as indicated in Fig. 9. Assume now that the uniform mode is excited at its resonance (as implied in Fig. 9). Since the density of states is higher near the upper edge of the band than near the lower edge, the line width should increase as ω_0 moves toward ω_2, and then suddenly decrease, as ω_0 goes beyond ω_2. For spherical samples this occurs at signal frequencies smaller than $(2/3)\omega_M$. These effects can readily be observed in experiments (60).

If the uniform mode is excited off-resonance, a diagram very similar to Fig. 9 applies, since the interacting spin waves now have the same frequency as the signal, regardless of the uniform mode frequency. In this case the inhomogeneity induced scattering leads to high effective damping of the uniform mode when the signal frequency lies inside the spin-wave band, and low effective damping, when the signal frequency lies outside the spin-wave band. This dependence of the effective damping (usually expressed in terms of an effective line width) has been studied experimentally in many material (61–64). The results are generally in good qualitative agreement with the theoretical predictions.

The quantitative predictions of the spin-wave theory (59) of anisotropy induced line width in polycrystals are that it should be proportional to H_a^2/M_s, and that it should have a characteristic frequency dependence, which is illustrated in Fig. 10 for spherical samples. In this graph, the ordinate is the line width divided by 26.01 times H_a^2/M_s. The solid line applies to materials with very large grain size, where the effect of exchange coupling does not influence the spin-wave frequencies significantly. The broken line takes account of the exchange correction for a representative grain size.

A detailed experimental test of these predictions has been carried out by Van Hook and Euler (65), who measured the line width for a class of garnet materials ($Y_{3-2x}Ca_{2x}Fe_{5-x-y}V_xIn_yO_{12}$), for which anisotropy field and saturation magnetization could be determined independently by measurements on single-crystals. Their results confirmed the validity of the theory over about two orders of magnitude of the anisotropy parameter H_a^2/M_s^2, but at both ends of this interval some discrepancies became noticeable. At low values of the anisotropy parameter the effect of porosity became dominant, and at high values the measured line width increased more gradually with the anisotropy parameter than expected from Ref. (59). The latter discrepancy can be attributed to the fact that the theory described in Ref. (59) is approximate in as much as it accounts only for the interaction of the uniform mode with the spin waves (primary scattering), but neglects the interaction between spin waves (secondary scattering). A more accurate theory, in which secondary scattering is also taken into account (66), gave better agreement with the measured data for large anisotropy parameters (65). The effect of porosity on line width was first pointed out in 1956 (67). This effect is similar to the line broadening due to surface roughness observed on polished spheres, and has been analyzed in detail by Sparks (48).

If the H_a/M_s ratio is very large, even the spin-wave theory that includes secondary scattering becomes inadequate. Under these conditions, the grains go through resonance independently. An appropriate theory for this case is described in Refs. (68) and (69). A somewhat surprising result of this independent-grain approach to FMR theory is the prediction that for a polycrystal with random grain orientation, the absorption spectrum has two separate peaks under certain

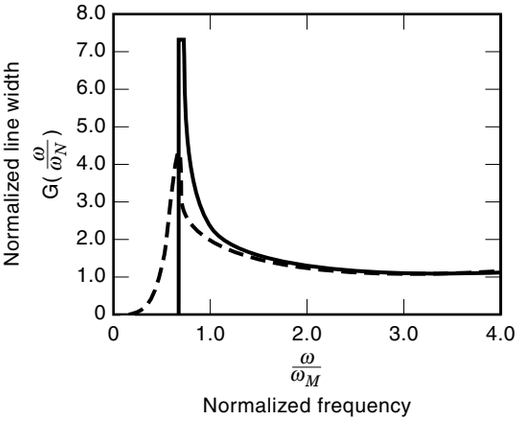

Figure 10. Theoretical frequency dependence of two-magnon line width.

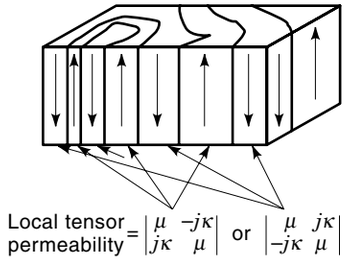

Figure 11. Representative arrangement of up and down domains for a single-crystal with uniaxial anisotropy.

conditions. Experimental verification of this prediction has been described by Zeender and Schloemann (70), using $NiFe_{1.3}Al_{0.7}O_4$, a low magnetization material with a large anisotropy field. An absorption spectrum having two separate peaks could also be caused by the excitation of the exchange resonance. This possibility was ruled out by the observation that both peaks of the spectrum were excited by the same sense of circular polarization.

Relating Microscopic Theories to Phenomenological Description of Damping

In this section we will briefly discuss how the phenomenological description of damping, introduced in a previous section, can be adapted to be consistent with the results of the microscopic theories. If the damping parameter α in Eqs. (2) and (3) is assumed to be constant, the resultant expressions for μ and κ would be at variance with the results of the microscopic theories. However, if α is taken to be a general function of frequency and internal magnetic bias field (as well as other material parameters) the expressions for μ and κ will substantially be in agreement with the microscopic theories. There would still be some minor discrepancies, such as the fact that the line shift induced by spin-wave interaction is neglected, and that the dependence of the spin-wave relaxation time on wavenumber is not included, but these shortcomings are of little importance in the analysis and design of ferrite microwave devices.

MICROWAVE BEHAVIOR OF PARTIALLY MAGNETIZED FERRITES

Many microwave devices, in particular phase shifters, use ferrite materials in a partially magnetized state, which is characterized by the z-component of magnetization (M_z) being smaller than M_s. For polycrystals with random easy-axis orientation, there are two distinct reasons for this reduction. First, the local magnetization vector tends to rotate and become aligned with the local easy axis, the more so, the smaller the internal magnetic field; and second, when the external magnetic field becomes smaller than the remanent magnetization times the demagnetizing factor, the magnetization of the individual grains breaks up into domains, each of these domains having easy-axis orientation. This is illustrated in Fig. 11, which shows a representative (but arbitrary) arrangement of domain walls in a single-crystal grain. The first of the magnetization processes mentioned is generally reversible, that is not associated with hysteresis, whereas the second one is associated with hysteresis.

The effect of the rotation process on the microwave permeability tensor can be taken into account by first finding the equilibrium direction of the local dc magnetization vector, then calculating the local susceptibility in the manner described previously, and finally averaging this local susceptibility over the easy-axis orientations present in the polycrystal. The most significant result of this procedure (which will be discussed further in the next section) is that the off-diagonal tensor component κ becomes proportional to M_z, rather than M_s. In the present section the rotational process will be disregarded, which is permissible, for instance, for a single-crystal magnetized in an easy direction.

Permeability of Partially Magnetized Ferrites

Consider now an arbitrary arrangement of up and down domains in a partially magnetized single-crystal ferrite, such as illustrated in Fig. 11. The local tensor permeability in the interior of the up domains is given by the expressions shown in Eqs. (8) and (9). Since the internal magnetic field is zero, ω_H in Eq. (9) is proportional to the anisotropy field. The local tensor permeability in the down domains is given by the same expression, except that the sign of κ is reversed. The question now arises: How can the macroscopic permeability, defined as the ratio of the spatial averages of magnetic induction and magnetic field, be calculated from this information? It turns out that the problem can be solved simply and explicitly if the domain pattern consists of a concentric array of circular shells (71) or of an array of parallel plates (72). By using the magnetostatic approximation, it can easily be shown in both cases that the components μ and κ of the macroscopic (sometimes also called global or effective) permeability tensor are related to the components μ_ℓ and κ_ℓ of the local permeability tensor by the condition

$$\mu^2 - \kappa^2 = \mu_\ell^2 - \kappa_\ell^2 \tag{47}$$

which implies that the two tensors have the same determinant. In Refs. 71 and 72, Eq. (47) was mathematically proved only for arrays of concentric shells or parallel plates, but a general proof has been given by Bouchaud and Zerah (73), based on earlier work by Mendelson (74).

A second relationship between the tensor components is

$$\kappa = \zeta \kappa_\ell \tag{48}$$

where ζ is the normalized magnetization of the partially magnetized ferrite ($-1 < \zeta < 1$). Eq. (48) is certainly plausible, and reduces to the right values for $\zeta = 1$ and -1, but it cannot be justified rigorously. Calculations based on the cylindrical shell model have shown that κ actually also depends on parameters other than the normalized magnetization ζ [see Figs. 4 and 10 of Ref. 71]. These other parameters have no simple physical significance, however, and therefore cannot readily be used for a representation of κ that might be more accurate than Eq. (48). Using Eqs. (48) and (47) together leads to a simple expression for the diagonal component of the macroscopic permeability tensor of a ferrite with an "up-and-down" domain structure, such as illustrated in Fig. 11.

$$\mu = [\mu_1^2 - \kappa_1^2(1 - \zeta^2)]^{1/2} \tag{49}$$

Consider now the demagnetized state, characterized by $\zeta = 0$. Using Eq. (9) one obtains by a straightforward calculation (again assuming an up-and-down domain configuration)

$$\mu = \{[(\omega_A + \omega_M + j\alpha\omega)^2 - \omega)^2]/[(\omega_A + j\alpha\omega)^2 - \omega^2]\}^{1/2} \quad (50)$$

Here ω_H in Eq. (9) has been replaced by $\omega_A = \gamma\mu_0 H_A$, since the effective bias field is entirely due to crystalline anisotropy. Note that simply inserting Eq. (9) into Eq. (49) leads to a more complicated version of Eq. (50), in which the numerator is a fourth order polynomial in ω. Equation (50) is obtained by cancelling the common factor. This equation can be generalized to make it applicable to demagnetized materials with random magnetization orientation, by noting that the permeability applicable with the RF field parallel to the domain magnetizations is (substantially) equal to unity. Thus, the isotropic permeability for a demagnetized material with random distribution of the magnetization orientations is

$$\mu = \tfrac{2}{3}\{[(\omega_A + \omega_M + j\alpha\omega)^2 - \omega^2]/[(\omega_A + j\alpha\omega)^2 - \omega^2]\}^{1/2} + \tfrac{1}{3} \quad (51)$$

If the losses are small and $\omega_A \ll \omega_M$, a condition frequently satisfied in typical microwave ferrites, this expression can be further simplified to

$$\mu = \tfrac{2}{3}[1 - (\omega_M/\omega)^2] + \tfrac{1}{3} \quad (52)$$

This formula has been shown to agree quite well with the experimental data on several ferrites over a wide range of frequencies (see Fig. 6 of Ref. 72).

Green and Sandy (75,76) have given a description of the techniques used for microwave measurements on partially magnetized ferrites and have summaried the results obtained in these measurements. Igarashi and Naito (77) have derived a theoretical expression for the parallel component μ_z of the permeability of partially magnetized ferrites, and have documented its agreement with relevant experimental data.

Low-Field Loss in Partially Magnetized Ferrites

It has been known since the early 1950s that partially magnetized ferrites are very lossy at frequencies smaller than a certain characteristic frequency that is substantially proportional to the saturation magnetization. Polder and Smit (78) pointed out that this "low-field loss" can be attributed to a gyromagnetic resonance, in which the magnetization vectors of oppositely polarized magnetic domains precess around the directions of the local dc magnetizations. The precessional motion gives rise to a divergence of the magnetization field at the domain walls, and hence to an RF stray field. Since this field is proportional to the saturation magnetization, the resonant frequency is expected to be proportional to the saturation magnetization.

The physical ideas proposed by Polder and Smit are quite consistent with the theory of partially magnetized ferrites, described in the preceding section, in which the magnetic structure is assumed to consist of "up and down" domains. This theory should therefore be considered to be a quantitative elaboration of their proposal. Inspection of Eq. (51) shows that it indeed predicts that μ has a large imaginary part (even in the limit of very small damping) when $\omega_A < \omega < \omega_A + \omega_M$. It may be concluded therefore that Eq. (51) describes the phenomenon of low-field loss in demagnetized ferrites at least qualitatively. For a quantitative comparison of experimental data with the theoretical predictions, see Ref. 72, Figs. 7–9.

An extension of the theory to the case of materials that are only partially demagnetized (i.e., $0 < \zeta < 1$) has been described in Ref. 79. The effect of dc magnetic field inhomogeneity on the observation and measurement of low-field loss is also discussed in this paper. An alternative quantitative theory of low-field loss, also based on the Polder and Smit proposal (78), has been advanced by Stitzer (80).

MATHEMATICAL MODELS OF POLYCRYSTALLINE FERRITES

For the analysis and design of ferrite microwave devices, the mathematical description of the material properties clearly plays a very important role. Until the mid-1990s, the design of (low-power) ferrite microwave devices was generally based on the formulas for the Polder tensor and its extension to lossy media [see Eqs. (8) and (9)]. Appropriate allowances were made for the reduction in the magnitude of the off-diagonal tensor component, when the material was only partially magnetized, and low-field loss was avoided by choosing materials with a sufficiently low saturation magnetization. However, an adequate mathematical model that would quantitatively take account of the low-field reduction of dc magnetization (and the associated reduction of κ), as well as take account of low-field loss was not available. Such a model would probably not even have been considered useful, because the design of ferrite microwave devices was largely an empirical art. With the advent of powerful computer programs that allow the solution of Maxwell's equations for the very complex geometries of interest in device design, it has become apparent that a realistic mathematical model, describing all aspects of the microwave behavior of ferrites (in particular polycrystalline ferrites), would be very useful. The most accurate solution of Maxwell's equations for a ferrite microwave device is of little value, unless it is based on a realistic representation of the microwave permeability of the ferrite material.

The conventional mathematical model of ferrite microwave materials is represented by the Polder permeability tensor, with damping included, as summarized in Eqs. (8) and (9). This model is not quite adequate because:

1. It fails to account for the (reversible) reduction of M_z at low internal fields, where $M_r < M_z < M_s$.
2. It does not apply when the material is "'irreversibly" demagnetized, either totally or partially ($M_z < M_r$), since low-field loss is neglected.
3. It may be misleading with respect to damping (unless α is taken to be a function of frequency, magnetic field, and other parameters).

In the preceding sections some of these shortcomings were already discussed and their resolution was outlined. The remaining task is to develop a (hopefully simple) mathematical procedure that can be used for calculating the permeability tensor more accurately and thus corrects the shortcomings of the conventional model.

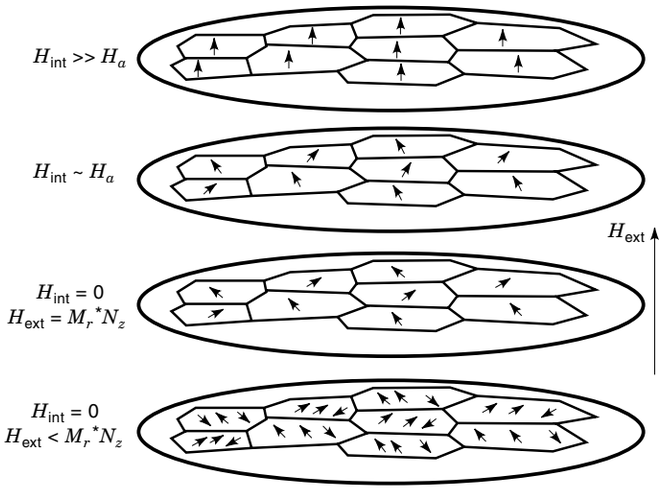

Figure 12. Distribution of magnetization in a polycrystal at four bias field strengths.

The mathematical model to be descibed here is based on the physical picture illustrated in Fig. 12, which shows qualitatively how the local magnetization vectors inside the grains of a polycrystal are oriented, as the magnetic field applied external to an ellipsoidal sample of ferrite is varied. If the external field is very large, the internal magnetic field will be large compared to the anisotropy field H_a, and all grain magnetizations become aligned with the field direction, as shown in the top diagram of Fig. 12. When the internal field is reduced to a value comparable to H_a the grain magnetizations will differ significantly from alignment with the field direction, their orientation being about halfway between the field direction and the closest easy-axis direction, as shown in the second diagram of Fig. 12. As the external field is reduced further, the internal field will approach zero, and the net magnetization approaches the remanent magnetization M_r, as illustrated in the third diagram of Fig. 12. Up to this point, most of the grains will remain uniformly magnetized, since it is energetically favorable, but when the external field is further reduced the grain magnetizations break up into domains, shown in the bottom diagram of Fig. 12 as having opposite polarity. The internal field remains at zero, or at some very small value in this regime.

Before the microwave permeability can be calculated, the dc magnetization has to be determined. For this purpose, the crystalline anisotropy energy must be considered. In cubic materials, such as spinels and garnets, the lowest order term of this energy (per unit volume) can be represented by (see for instance Ref. 14)

$$E_{anis} = K_1(a_1^2a_2^2 + a_2^2a_3^2 + a_3^2a_1^2) \tag{53}$$

where a_1, a_2, a_3 are the directional cosines of the magnetization with respect to the cubic axes. If K_1 is positive, the energy minimum occurs at the [100] direction, if K_1 is negative (as for most ferrites), it occurs at the [111] direction. Figure 13 shows the contours of constant anisotropy energy on the surface of a unit sphere. Any direction of the magnetization vector is represented by a point on the sphere surface. Only one octant of the sphere surface is shown, because the identical pattern is repeated in every other octant. For each contour shown in this diagram the normalized energy E_n has the constant values shown in the inset. Here, the normalized energy is the direction-dependent, second factor on the right hand side of Eq. (53), except that a constant has been subtracted, reducing the normalized energy to zero for the [111] direction. Assume now that the sample is a polycrystal with random grain orientation. The bias field direction for any grain can be represented by a point in the diagram of Fig. 13. For high field strength the magnetization is aligned with the field direction. As the field is reduced, the grain magnetization rotates to the closest [111] direction. The calculation of dc magnetization and RF permeability can in principle be based on this physical picture, but such a calculation would be quite complicated. Much simpler results are obtained, if we consider the case in which the easy axes of all grains are misaligned by the same polar angle relative to the bias field direction, and the azimuth angles are distributed randomly. For simplicity, we will also approximate the actual angular dependence of the anisotropy energy by a uniaxial dependence that matches it near the energy minimum.

Consider now a single-crystal grain, with an easy axis oriented at an angle θ_0 to the direction of the bias field, and a magnetization direction characterized by a polar angle θ and azimuth angle ϕ, as shown in Fig. 14. The magnetization vector then includes an angle ψ with the easy axis, where ψ is given by

$$\cos\psi = \cos\theta_0\cos\theta + \sin\theta_0\sin\theta\cos(\phi_0 - \phi) \tag{54}$$

The magnetic energy density in an internal magnetic field H_{int} is given by

$$E = \mu_0 M_s[\tfrac{1}{2}H_a(1 - \cos^2\psi) - H_{int}\cos\theta] \tag{55}$$

The conditions for a minimum of this energy are readily found to be

$$\phi = \phi_0 \quad H_{int}/H_a = \tfrac{1}{2}\sin[2(\theta_0 - \theta)]/\sin\theta \tag{56}$$

Since the normalized z-component of magnetization is $M_z/M_s = \cos\theta$, Eq. (56) can readily be used to calculate M_z as a function of H_{int}, for given remanence ratio $R_m = M_r/M_s$ (which is simply related to the misalignment angle θ_0). Figure 15 shows the resulting dependence of magnetization on internal magnetic field.

After determining the dc magnetic state of the ferrite in the manner described above, calculation of the RF permeability is straightforward as long as the grains remain magnetized to saturation (i.e., $H_{int} > 0$). For this purpose, the permeability tensor is first calculated in a coordinate system aligned with the direction of the local dc magnetization. This local permeability is then transformed to a coordinate system aligned with the bias field, and an average is taken over the azimuth angle. The resulting expression for the permeability tensor has the same form as the Polder tensor [see Eq. (8)], but the off-diagonal element of the tensor is reduced in magnitude.

The permeability tensor applicable when M_z is less than M_r can be calculated in similar fashion by using the results obtained previously, expressing them in a rotated coordinate system, and averaging over the azimuth angle. In this context

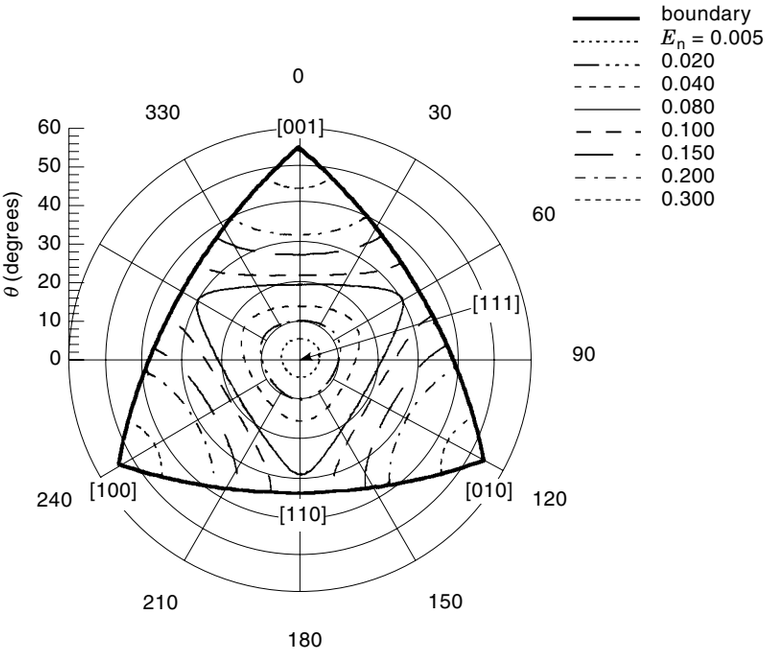

Figure 13. Contours of constant anisotropy energy for $K_1 < 0$.

it is important to realize that in this regime the microwave permeability is not a function of the internal magnetic bias field, which is zero under these conditions (or at least very small). Two options are available for displaying the microwave permeability as a function of magnetic bias field in this case. The permeability can be plotted as a function of external magnetic bias field (for given demagnetizing factor), or it can be plotted on a dual-scale graph as a function of H_{int} for $M_z > M_r$, and as a function of $\zeta = M_z/M_r$ for $M_z < M_r$.

A FORTRAN subroutine has been developed that calculates all components of the microwave permeability tensor, based on the procedure outlined previously (81). For simplicity, the effective line width is assumed to be a linear function of frequency (i.e., a constant term plus a term proportional to frequency). As explained, the actual dependence of effective line width on signal frequency and internal bias field is a more complicated relationship that depends on the location of the signal frequency relative to the spin wave band. This dependence is not taken into account in the current version of the program, but will be included in future versions, together with other refinements. The essential inputs required for the subroutine are: saturation magnetization M_s, remanence ratio $R_m = M_r/M_s$, anisotropy field H_a, Gilbert damping constant α (which gives rise to an effective line width contribution that is proportional to frequency), frequency-independent contribution to the effective line width Δf_0, signal frequency, and internal dc bias field H_{int} or normalized magnetization $\zeta = M/M_r$. For convenience all input parame-

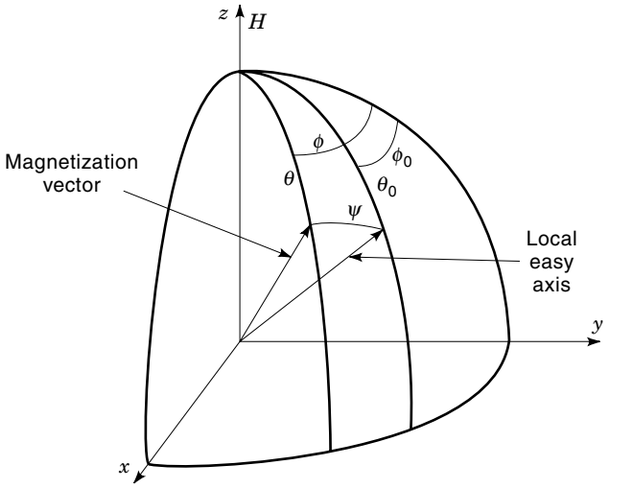

Figure 14. Conventions used for calculating dc magnetization and RF permeability.

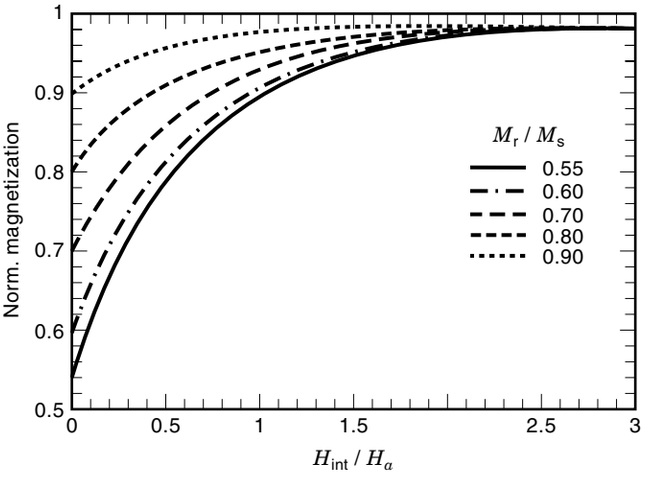

Figure 15. Calculated magnetization curve for a polycrystal.

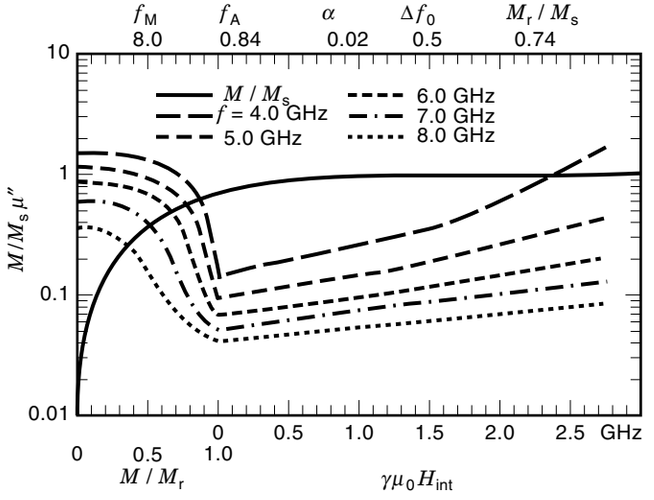

Figure 16. Low-field loss and dc magnetization, normalized magnetization, and μ'' vs. H_{int} and M/M_r.

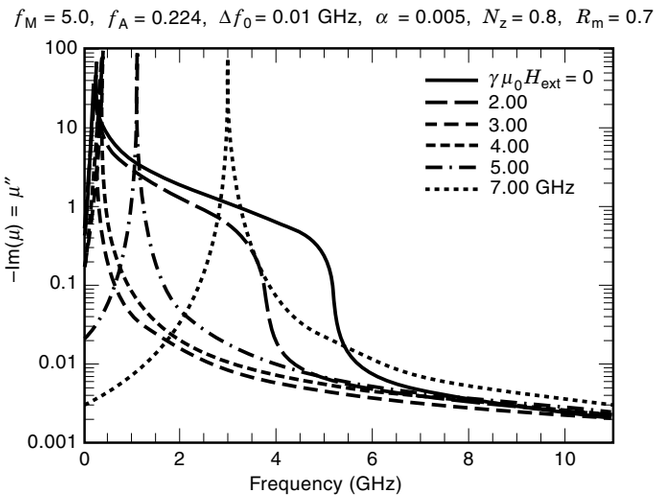

Figure 18. Low-field loss and FMR loss, μ'' vs. frequency for given H_{ext}.

ters are expressed either as pure numbers (remanence ratio, demagnetizing factor, Gilbert damping constant), or in terms of a characteristic frequency (in gigahertz). Examples of the latter are

$$f_A = \gamma\mu_0 H_a,\ f_M = \gamma\mu_0 M_s,\ f_H = \gamma\mu_0 H_{\text{int}},\ \Delta f_0 = \gamma\mu_0 \Delta H_{eff0} \quad \text{with} \quad \gamma = \gamma/2\pi \tag{57}$$

Figures 16–18 show some examples of the use of this mathematical model for calculating the magnetic loss (μ'') under various conditions. In Fig. 16, μ'' is shown on a dual scale as a function of internal bias field (on the right) and as a function of normalized magnetization (on the left). The reduced dc magnetization M/M_s is also shown as a function of the same variables. The assumed parameter values, which correspond to a material with relatively high saturation magnetization, are indicated at the top of the graph. Similar results, but for a different material, are summarized in Fig. 17. In this case μ'' is shown as a function of external bias field, assuming a demagnetizing factor of 0.8, for a material similar to YIG. For the same material, Fig. 18 shows the calculated dependence of μ'' on frequency for given values of external field. The results shown in these graphs are in qualitative agreement with the observations on typical microwave ferrites. The mathematical model used for the calculations is quite flexible, thus allowing one to adjust the various parameters such that good quantitative agreement with experimental data can be obtained.

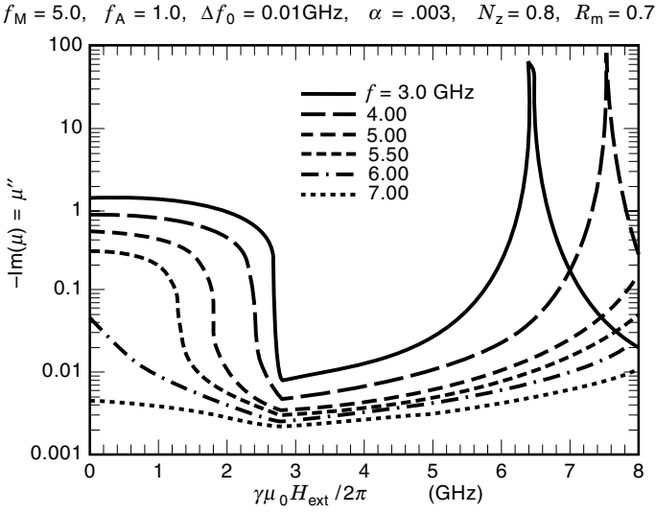

Figure 17. Low-field loss and FMR loss, μ'' vs. H_{ext} for given frequency.

In order to use this mathematical model for the analysis and design of microwave ferrite devices, the dc magnetization and internal magnetic bias field must first be determined. Even though the external bias field is frequently approximately uniform, the internal is usually quite nonuniform due to the nonuniform demagnetizing field. In some approaches to ferrite device design, the ferrite sample is conceptually subdivided into several parts, each of which has approximately the same microwave behavior. For instance, in the case of circulators, the junction disk may be subdivided into concentric rings and a central disk, with each of these parts having similar microwave behavior when the bias field is supplied by a disk-shaped magnet, as discussed in more detail in Refs. 82 and 83.

An alternative mathematical model of microwave ferrites has been proposed by Gelin and Berthou-Pichavant (84), who have stressed that a model based on causality is required when numerical time-domain methods are used for device design. In their model, the local anisotropy is represented by an anisotropy field, and all directions of this field are assumed to be equiprobable. Reasonably good agreement with relevant experimental data is documented.

BIBLIOGRAPHY

1. L. Néel, Magnetic properties of ferrites; ferromagnetism and antiferromagnetism (in French), *Ann. Phys.,* **3**: 137–198, 1948.

2. J. L. Snoek, *New Developments in Ferromagnetic Materials,* New York: Elsevier, 1947.
3. J. Smit and H. P. J. Wijn, *Ferrites,* New York: Wiley, 1959.
4. C. L. Hogan, The ferromagnetic Faraday effect at microwave frequencies and its applications, *Bell Syst. Tech. J.,* **31**: 1–31, 1952.
5. C. Kittel, *Introduction to Solid State Physics,* chap. 14, New York: Wiley, 1986.
6. B. Lax and K. J. Button, *Microwave Ferrites and Ferrimagnetics,* New York: McGraw-Hill, 1962.
7. A. G. Gurevich and G. A. Melkov, *Magnetization Oscillations and Waves,* Boca Raton, FL: CRC Press, 1996.
8. M. A. Gilleo, Ferromagnetic insulators: Garnets, chap. 1, and J. Nicholas, Microwave ferrites, chap. 2, in E. P. Wohlfarth (ed.), *Ferromagnetic Materials,* Amsterdam: North Holland, 1980.
9. G. P. Rodrigue, A generation of microwave ferrite devices, *Proc. IEEE,* **76**: 121–137, 1988.
10. F. Bertaut and F. Forrat, Structure of ferrimagnetic rare-earth ferrites (in French), *Compt. Rend., Paris,* **242**: 382–384, 1956.
11. S. Geller and M. A. Gilleo, Structure and ferrimagnetism of yttrium and rare-earth-iron garnets, *Acta Cryst.,* **10**: 239, 787, 1957.
12. G. Winkler, *Magnetic Garnets,* Braunschweig, Germany: F. Vieweg, 1981.
13. Y. Akaiwa and T. Okazaki, An application of a hexagonal ferrite to a millimeter-wave *Y* circulator, *IEEE Trans. Magn.* **10**: 374, 1974.
14. J. A. Weiss, N. G. Watson, and G. F. Dionne, New uniaxial-ferrite millimeter-wave junction circulator, paper C-2, *IEEE MTT/S Microw. Symp.,* Long Beach, CA, 1989; *Appl. Microw. Magn.,* 1990, pp. 74–85.
15. D. C. Webb, Microwave magnetic thin-film devices, *IEEE Trans. Magn.* **24**: 2799–2804, 1988.
16. J. R. Truedson et al., High-field effective linewidth and eddy-current losses in moderate conductivity single-crystal *M*-type barium hexagonal ferrite discs at 10–60 GHz, *J. Appl. Phys.,* **74**: 2705–2718, 1993.
17. P. C. Dorsey et al., Epitaxial yttrium iron garnet films grown by pulsed laser deposition, *J. Appl. Phys.,* **74**: 1242–1246, 1993.
18. P. C. Dorsey et al., Oriented barium hexaferrite thick films grown on *C*-plane and *M*-plane sapphire substrates, *IEEE Trans. Magn.,* **30**: 4512–4517, 1994.
19. H. Buhay et al., Thick yttrium-iron-garnet (YIG) films produced by pulsed laser deposition (PLD) for integration applications, *IEEE Trans. Magn.,* **31**: 3832, 1995.
20. J. D. Adam et al., *K*-band circulators on semiconductor wafers, *IEEE Intern. Microw. Symp.,* Paper TU1E-2, p. 227, 1996.
21. M. Abe and Y. Tamaura, Ferrite plating in aqueous solution: New technique for preparing magnetic thin films, *J. Appl. Phys.,* **55**: 2614–2616, 1984.
22. C. M. Williams et al., The magnetic and structural properties of ferrite plated Ni Zn-ferrite films, *IEEE Trans. Magn.,* **30**: 4896–4899, 1994.
23. M. Abe et al., Ultrasound enhanced ferrite plating: Bringing breakthrough in ferrite coating synthesized from aqueous solution, *IEEE Trans. Magn.,* **33**: 3649–3651, 1997.
24. A. M. Morrish, *The Physical Principles of Magnetism,* New York: Wiley, 1965.
25. W. H. Von Aulock, *Handbook of Microwave Ferrite Materials,* New York: Academic, 1965.
26. L. D. Landau and E. M. Lifshitz, On the theory of the dispersion of magnetic permeability in ferromagnetic bodies, *Phys. Zeitschrift Soviet U.,* **8**: 153, 1935.
27. T. L. Gilbert and J. M. Kelley, Anomalous rotational damping in ferromagnetic sheets, *Proc. 1st Conf. Magn. Magn. Mater.,* Pittsburgh: Amer. Inst. Electr. Eng., New York: p. 253, 1955.
28. D. Polder, On the theory of ferromagnetic resonance, *Philos. Magn.,* **40** (300): 99, 1949.
29. S. Foner, Antiferromagnetic and ferrimagnetic resonance, chap. 9 in *Magnetism, A Treatise on Modern Theory and Materials,* G. T. Rado and H. Suhl, (eds.), New York: Academic Press, vol. 1, 1963, p. 383.
30. N. Bloembergen and R. W. Damon, Relaxation effects in ferromagnetic resonance, *Phys. Rev.,* **85**: 699, 1952.
31. R. W. Damon, Relaxation effects in ferromagnetic resonance, *Rev. Mod. Phys.,* **25**: 239, 1953.
32. N. Bloembergen and S. Wang, Relaxation effects in para- and ferromagnetic resonance, *Phys. Rev.,* **93**: 72, 1954.
33. H. Suhl, The nonlinear behavior of ferrites at high microwave signal levels, *Proc. IRE,* **44**: 1270, 1956, and The theory of ferromagnetic resonance at high signal powers, *J. Phys. Chem. Solids,* **1**: 209, 1957.
34. R. W. Damon, Ferromagnetic resonance at high power, chap. 11 in *Magnetism, A Treatise on Modern Theory and Materials,* vol. 1, G. T. Rado and H. Suhl, (eds.), New York: Academic Press, 1963, p. 551.
35. E. Schloemann, J. J. Green, and U. Milano, Recent developments in ferromagnetic resonance at high power levels, *J. Appl. Phys.,* **31**: 386S, 1960.
36. J. J. Green and E. Schloemann, Ferromagnetic relaxation at low microwave frequencies, *J. Appl. Phys.,* **32**: 168S, 1961.
37. E. Schloemann and R. I. Joseph, Instability of spin waves and magnetostatic modes in a microwave magnetic field applied parallel to the dc field, *J. Appl. Phys.,* **32**: 1006, 1961.
38. T. Holstein and H. Primakoff, Field dependence of the intrinsic domain magnetization of a ferromagnet, *Phys. Rev.,* **58**: 1098, 1940.
39. E. Schloemann and J. J. Green, Spin-wave growth under parallel pumping, *J. Appl. Phys.,* **34**: 1291, 1963.
40. R. I. Joseph and E. Schloemann, Transient and steady-state absorption of microwave power under parallel pumping, *J. Appl. Phys.,* **38**: 1915, 1967.
41. E. Schloemann, Transient growth of spin waves in the presence of parametric excitation, *Bull., Acad. Sci. USSR, Phys. Series,* **28** (3): 454, 1964. English Version, p. 366, Columbia Technical Translations.
42. M. I. Kaganov and V. M. Tsukernik, Nonresonance absorption of the energy of an alternating magnetic field by a ferromagnetic dielectric, *Soviet Phys. JETP,* **37**: 587, 1960.
43. C. P. Hartwig et al., Subthreshold steady-state absorption under parallel pumping, *J. Appl. Phys.,* **36**: 1265, 1965.
44. T. Kohane and E. Schloemann, dc magnetic moment induced by a strong RF magnetic field applied parallel to the dc field, *J. Appl. Phys.,* **34**: 1544, 1963.
45. E. Schloemann, R. I. Joseph, and I. Bady, Spin-wave instability in hexagonal ferrites with a preferential plane, *J. Appl. Phys.,* **34**: 672, 1963.
46. C. Kittel and E. Abrahams, Relaxation processes in ferromagnetism, *Rev. Mod. Phys.,* **25**: 233, 1953.
47. A. M. Clogston et al., Ferromagnetic resonance line width in insulating materials, *J. Phys. Chem. Solids,* **1**: 129, 1956.
48. M. Sparks, *Ferromagnetic Relaxation Theory,* New York: McGraw-Hill, 1964.
49. C. W. Haas and H. B. Callen, Ferromagnetic relaxation and resonance line widths, chap. 10 in *Magnetism, A Treatise on Modern Theory and Materials,* G. T. Rado and H. Suhl (eds.), New York: Academic, **1**: p. 449, 1963.

50. H. Callen, A ferromagnetic dynamic equation, *J. Phys. Chem. Solids,* **4**: 256, 1958.
51. A. I. Akhiezer, Theory of relaxation processes in ferromagnetics at low temperatures, *J. Phys. (USSR),* **10**: 217, 1946.
52. T. Kasuya, The relaxation process in ferromagnetic resonance absorption, *Progr. Theoret. Phys. (Kyoto),* **12**: 802, 1954.
53. M. Sparks and C. Kittel, Ferromagnetic relaxation mechanism for M_z in Yttrium iron garnet, *Phys. Rev. Letters,* **4**: 232, 1960.
54. E. Schloemann, Ferromagnetic relaxation caused by interaction with thermally excited magnons, *Phys. Rev.,* **121**: 1312, 1961.
55. M. Sparks, R. Loudon, and C. Kittel, Ferromagnetic relaxation, 1, *Phys. Rev.,* **122**: 791, 1961.
56. A. I. Akhiezer, V. G. Bar'yakhtar, and S. V. Peletminskii, *Spin waves,* Amsterdam, North Holland: 1968.
57. B. Lamaire, H. Le Gall, and J. L. Dormann, Splitting of parametric magnons in ferromagnetic crystals, *Solid State Commun.,* **5**: 499, 1967.
58. T. Kasuya and R. C. Le Craw, Relaxation mechanisms in ferromagnetic resonance, *Phys. Rev. Letters,* **6**: 223, 1961.
59. E. Schloemann, Spin-wave analysis of ferromagnetic resonance in polycrystalline ferrites, *J. Phys. Chem. Solids,* **6**: 242, 1958.
60. C. R. Buffler, Ferromagnetic resonance near the upper limit of the spin wave manifold, *J. Appl. Phys.,* **30**: 172S, 1959.
61. C. E. Patton, Effective linewidth due to porosity and anisotropy in polycrystalline YIG and Ca-V substituted YIG at 10 GHz, *Phys. Rev.,* **179**: 352, 1969.
62. T. Kohane and E. Schloemann, Linewidth and off-resonance loss in polycrystalline ferrites at microwave frequencies, *J. Appl. Phys.,* **39**: 720, 1968.
63. Q. H. F. Vrehen, Absorption and dispersion in porous and anisotropic polycrystalline ferrites at microwave frequencies, *IEEE Trans. Magn.,* **MAG-4**: 479, 1968.
64. R. Karim et al., Frequency dependence of the ferromagnetic resonance linewidth and effective linewidth in manganese substituted single-crystal barium ferrite, *J. Appl. Phys.,* **73**: 4512, 1993.
65. H. J. Van Hook and F. Euler, Anisotropy linebroadening in polycrystalline V-In substituted YIG, *J. Appl. Phys.,* **40**: 4001, 1969.
66. E. Schloemann, Inhomogeneous broadening of ferromagnetic resonance lines, *Phys. Rev.,* **182**: 632, 1969.
67. E. Schloemann, The microwave susceptibility of polycrystalline ferrites in strong dc fields and the influence of nonmagnetic inclusions on the microwave susceptibility, *Proc. 2nd Conf. Magn. Magn. Mater.,* Boston: Amer. Inst. of Electr. Eng. Pub., T-91, 1957, pp. 600–609.
68. E. Schloemann, Ferromagnetic resonance in polycrystalline ferrites with large anisotropy, *J. Phys. Chem. Solids,* **6**: 257, 1958.
69. E. Schloemann and R. V. Jones, Ferromagnetic resonance in polycrystalline ferrites with hexagonal crystal structure, *J. Appl. Phys.,* **30**: 177S, 1959.
70. R. J. Zeender and E. Schloemann, Ferromagnetic resonance in polycrystalline ferrites using circularly polarized radiation, *J. Appl. Phys.,* **31**: 1112, 1960.
71. E. Schloemann, Microwave behavior of partially magnetized ferrites, *J. Appl. Phys.,* **41**: 204–214, 1970.
72. E. Schloemann, Behavior of ferrites in the microwave frequency range, *J. Physique (France)* **32**: C1-443–C1-451, 1971.
73. J. P. Bouchaud and P. G. Zerah, Spontaneous resonances and universal behavior in ferrimagnetics: Effective medium theory, *Phys. Rev. Lett.,* **63**: 1000–1003, 1989.
74. K. S. Mendelson, Effective conductivity in two-phase material with cylindrical phase boundaries, *J. Appl. Phys.,* **46**: 917–918, 1975.
75. J. J. Green and F. Sandy, Microwave characterization of partially magnetized ferrites, *IEEE Trans. Microw. Theory Tech.,* **22**: 641–645, 1974.
76. J. J. Green and F. Sandy, A catalog of low-power loss parameters and high-power thresholds for partially magnetized ferrites, *IEEE Trans. Microw. Theory Tech.,* **22**: 645–651, 1974.
77. M. Igarashi and Y. Naito, Parallel component μ_z of partially magnetized microwave ferrites, *IEEE Trans. Microw. Theory Tech.,* **29**: 568–571, 1981.
78. D. Polder and J. Smit, Resonance phenomena in ferrites, *Rev. Mod. Phys.,* **25**: 89–90, 1953.
79. E. Schloemann, Theory of low-field loss in partially magnetized ferrites, *IEEE Trans. Magn.,* **28**: 3300–3302, 1992.
80. S. Stitzer, Modeling a stripline ferrite phase shifter, Paper We4 F3, presented at *Int. Microw. Symp.,* Denver, 1997.
81. E. Schloemann, Mathematical models of microwave ferrites, *J. Phys. VI France,* **7**: C1-433, 1997. *Proc. 7th Int. Conf. Ferrites,* Bordeaux: Sept. 1996.
82. E. Schloemann, Integrated dc/RF design of dual-ferrite circulators, *IEEE Trans. Magn.,* **33**: 3430–3432, 1997.
83. E. Schloemann, Integrated dc/RF design theory for ferrite circulators, *J. Appl. Phys.,* **81**: 5070–5072, 1997.
84. P. Gelin and K. Berthou-Pichavant, New consistent model for ferrite permeability tensor with arbitrary magnetization state, *IEEE Trans. Microw. Theory Tech.,* **45**: 1185–1192, 1997.

ERNST F. SCHLOEMANN
Consultant